



# Small-Scale Geochemical Heterogeneities and Seasonal Variation of Iron and Sulfide in Salt Marshes Revealed by Two-Dimensional Sensors

OPEN ACCESS

**Edited by:**

Natascha Riedinger,  
Oklahoma State University,  
United States

**Reviewed by:**

Vincent Noel,  
Stanford University, United States  
Sophia LaFond-Hudson,  
Oak Ridge National Laboratory (DOE),  
United States

**\*Correspondence:**

Qingzhi Zhu  
qing.zhu@stonybrook.edu  
J. Kirk Cochran  
kirk.cochran@stonybrook.edu

**† Present Address:**

Joseph J. Tamborski,  
Department of Ocean and Earth  
Sciences, Old Dominion University,  
Norfolk, VA, United States

**Specialty section:**

This article was submitted to  
Biogeoscience,  
a section of the journal  
Frontiers in Earth Science

**Received:** 15 January 2021

**Accepted:** 06 April 2021

**Published:** 29 April 2021

**Citation:**

Zhu Q, Cochran JK, Heilbrun C,  
Yin H, Feng H, Tamborski JJ,  
Fitzgerald P and Cong W (2021)  
Small-Scale Geochemical  
Heterogeneities and Seasonal  
Variation of Iron and Sulfide in Salt  
Marshes Revealed by  
Two-Dimensional Sensors.  
Front. Earth Sci. 9:653698.  
doi: 10.3389/feart.2021.653698

Qingzhi Zhu<sup>1\*</sup>, J. Kirk Cochran<sup>1\*</sup>, Christina Heilbrun<sup>1</sup>, Hang Yin<sup>1</sup>, Huan Feng<sup>2</sup>,  
Joseph J. Tamborski<sup>3†</sup>, Patrick Fitzgerald<sup>1</sup> and Wen Cong<sup>1</sup>

<sup>1</sup> School of Marine and Atmospheric Sciences, Stony Brook University, Stony Brook, NY, United States, <sup>2</sup> Department of Earth and Environmental Studies, Montclair State University, Montclair, NJ, United States, <sup>3</sup> Department of Geosciences, Stony Brook University, Stony Brook, NY, United States

Loss of tidal wetlands is a world-wide phenomenon. Many factors may contribute to such loss, but among them are geochemical stressors such as exposure of the marsh plants to elevated levels on hydrogen sulfide in the pore water of the marsh peat. Here we report the results of a study of the geochemistry of iron and sulfide at different seasons in unrestored (JoCo) and partially restored (Big Egg) salt marshes in Jamaica Bay, a highly urbanized estuary in New York City where the loss of salt marsh area has accelerated in recent years. The spatial and temporal 2-dimensional distribution patterns of dissolved Fe<sup>2+</sup> and H<sub>2</sub>S in salt marshes were *in situ* mapped with high resolution planar sensors for the first time. The vertical profiles of Fe<sup>2+</sup> and hydrogen sulfide, as well as related solutes and redox potentials in marsh were also evaluated by sampling the pore water at discrete depths. Sediment cores were collected at various seasons and the solid phase Fe, S, N, C, and chromium reducible sulfide in marsh peat at discrete depths were further investigated in order to study Fe and S cycles, and their relationship to the organic matter cycling at different seasons. Our results revealed that the redox sensitive elements Fe<sup>2+</sup> and S<sup>2-</sup> showed significantly heterogeneous and complex three dimensional distribution patterns in salt marsh, over mm to cm scales, directly associated with the plant roots due to the oxygen leakage from roots and redox diagenetic reactions. We hypothesize that the oxic layers with low/undetected H<sub>2</sub>S and Fe<sup>2+</sup> formed around roots help marsh plants to survive in the high levels of H<sub>2</sub>S by reducing sulfide absorption. The overall concentrations of Fe<sup>2+</sup> and H<sub>2</sub>S and distribution patterns also seasonally varied with temperature change. H<sub>2</sub>S level in JoCo sampling site could change from <0.02 mM in spring to >5 mM in fall season, reflecting significantly seasonal variation in the rates of bacterial oxidation of organic matter at this marsh site. Solid phase Fe and S showed that very high fractions of the diagenetically

reactive iron at JoCo and Big Egg were associated with pyrite that can persist for long periods in anoxic sediments. This implies that there is insufficient diagenetically reactive iron to buffer the pore water hydrogen sulfide through formation of iron sulfides at JoCo and Big Egg.

**Keywords:** salt marsh geochemistry, planar optical sensors, Jamaica Bay, 2-D distributions,  $\text{Fe}^{2+}$  and  $\text{H}_2\text{S}$

## INTRODUCTION

The worldwide loss of salt marsh wetlands has been linked to many factors, including sea level rise, coastal development, coastal eutrophication and geochemical stressors. Salt marshes need to accrete to keep pace as sea level rises. Marsh accretion is affected by growth of the plants, accumulation of organic matter and lithogenic particles and formation of authigenic phases (e.g.,  $\text{Fe}_2\text{S}$ ) in marsh peat. Cycling of iron compounds, hydrogen sulfide ( $\text{H}_2\text{S}$ ) and nutrients N and P could provide stress on salt marsh plants. Hydrogen sulfide is known as a toxin to marsh plants (Kolker, 2005; Lamers et al., 2013; Alldred et al., 2020), and addition of nutrients and organic matter to marshes may enhance hydrogen sulfide production (Kolker, 2005). The input of iron particles on marsh may increase marsh accretion by reducing dissolved  $\text{H}_2\text{S}$  and forming the mineral pyrite in the marsh. But previous results also imply that the marsh biomass could be degraded if iron in marsh is too high and causes removal of the nutrient phosphorus (Cochran et al., 2018). Therefore, understanding the distribution patterns and seasonal variations of iron and sulfide in salt marshes, as well as possible geochemical constraints on salt marsh loss, is critical for the study of marsh health and resiliency.

Iron (Fe) and sulfur (S) are two important redox-sensitive elements in salt marshes, their distribution patterns with depth reflect multiple biogeochemical reactions and processes in the deposits, for example, organic matter decomposition, sulfate reduction/sulfide oxidation, availability of reactive Fe, and accumulation rate of authigenic pyrite minerals (Berner, 1984; Canfield et al., 1992; Goldhaber, 2003; Jørgensen and Nelson, 2004; Jørgensen and Kasten, 2006; Aller et al., 2010; Luther et al., 2011). All these biogeochemical processes are closely coupled to the environment and ecosystem of salt marshes, including marsh peat degradation, accretion, biomass growth/decline, and species diversities (Luther and Church, 1988; Kostka and Luther, 1995; Sundby et al., 2003; Luo et al., 2017).

Particulate Fe is typically input to coastal marshes through wind-blown dust, river run-off, and tidal flooding. The oxidized Fe-containing mineral particles directly deposit on the marsh surface, and subsequently become involved in early diagenetic reactions in marsh peat. One important pathway for Fe cycling in marsh is microbial iron reduction, a common pathway of  $\text{Fe}^{3+}$ -oxides reduction to  $\text{Fe}^{2+}$  by organic matters mediated by  $\text{Fe}^{3+}$ -reducing microorganisms (Weiss et al., 2005; Luo et al., 2015, 2016, 2017). In sulfidic zones,  $\text{Fe}^{3+}$ -oxide minerals can also abiotically react with sulfide to produce dissolved  $\text{Fe}^{2+}$ , which subsequently react with sulfide, generating the authigenic minerals FeS and pyrite ( $\text{FeS}_2$ ) (Berner, 1970; Canfield, 1989; Kostka and Luther, 1995). Hydrogen sulfide in marsh pore water

is generally produced from the reduction of sulfate by bacteria as organic matter is oxidized. Because of the large amount of labile organic matter in marshes (e.g., from marsh plants or combined sewer overflows), the active electron acceptors  $\text{O}_2$ , nitrate/nitrite, Mn/Fe-oxide could be completely consumed by organic matter within a very thin surficial layer of the marsh peat, resulting in an anoxic sulfidic environment in most salt marshes. Under anoxic conditions, sulfate-reducing bacteria use  $\text{SO}_4^{2-}$  as an electron acceptor for organic matter remineralization, generating  $\text{H}_2\text{S}$  as one of the end products (Goldhaber, 2003; Jørgensen and Nelson, 2004). This anaerobic respiration process often dominates in organic matter-rich salt marshes, resulting in high concentrations of dissolved sulfide at millimolar (mM) levels (Bagarinao, 1992).  $\text{H}_2\text{S}$ , one specie of the total dissolved sulfide ( $\Sigma \text{H}_2\text{S} = [\text{H}_2\text{S}] + [\text{HS}^-] + [\text{S}^{2-}]$ ), is harmful to marsh plants such as *Spartina alterniflora*. Long-term exposures to levels greater than  $\sim 4$  mM  $\text{H}_2\text{S}$  in marsh pore water can cause plant die-off, and subsequent peat degradation and subsidence (Kolker, 2005; Cochran et al., 2013; Lamers et al., 2013).

Typically, the intense redox reactions and precipitation/dissolution reactions in the surficial marsh peat generate sharp gradients of  $\text{Fe}^{2+}$  and  $\text{H}_2\text{S}$  in marsh pore water. The  $\text{H}_2\text{S}$  concentrations can increase from 0 to several mM over depths of millimeters to centimeters, with the concentrations of  $\text{Fe}^{2+}$  changing by several hundred micromolar ( $\mu\text{M}$ ). The compositional changes with depth in deposits are usually assumed steady and to occur in an overall average vertical progression. However, the growth of marsh plants and the activities of dwelling fauna can generate significant heterogeneity and complex three dimensional reaction patterns of Fe and S over millimeter to meter scales due to plant rhizosphere development, oxygen transport through roots, burrow construction, and bioirrigation (Aller, 1982, 2001; Sundby et al., 2003; Weiss et al., 2005). The seasonal cycling of Fe and S in salt marsh sediments have been reported (Luther et al., 1986; Kostka and Luther, 1995; Luo et al., 2017), and 2-D distributions of dissolved  $\text{Fe}^{2+}$  and  $\text{H}_2\text{S}$  in coastal marine sediments have also been discussed elsewhere (Zhu and Aller, 2012, 2013; Yin et al., 2017). However, the small scale 2-D distribution patterns of dissolved  $\text{Fe}^{2+}$  and  $\text{H}_2\text{S}$  associated with the plant rhizosphere in salt marshes have not been investigated so far. *In situ* measurements of real-time, high-resolution 2-D distributions of  $\text{H}_2\text{S}$  and  $\text{Fe}^{2+}$  around plant roots may provide insight into the nature of interactions between the oxygen, iron, and sulfur cycles in marsh plant rhizosphere.

Jamaica Bay, New York has suffered considerable loss of salt marsh acreage over the past  $\sim 50$  years. A large unrestored marsh island JoCo and a partially restored marsh island Big Egg were selected as study sites in this work. We noted that the  $\text{H}_2\text{S}$  levels at JoCo marsh could be elevated to  $>6$  mM in summer and

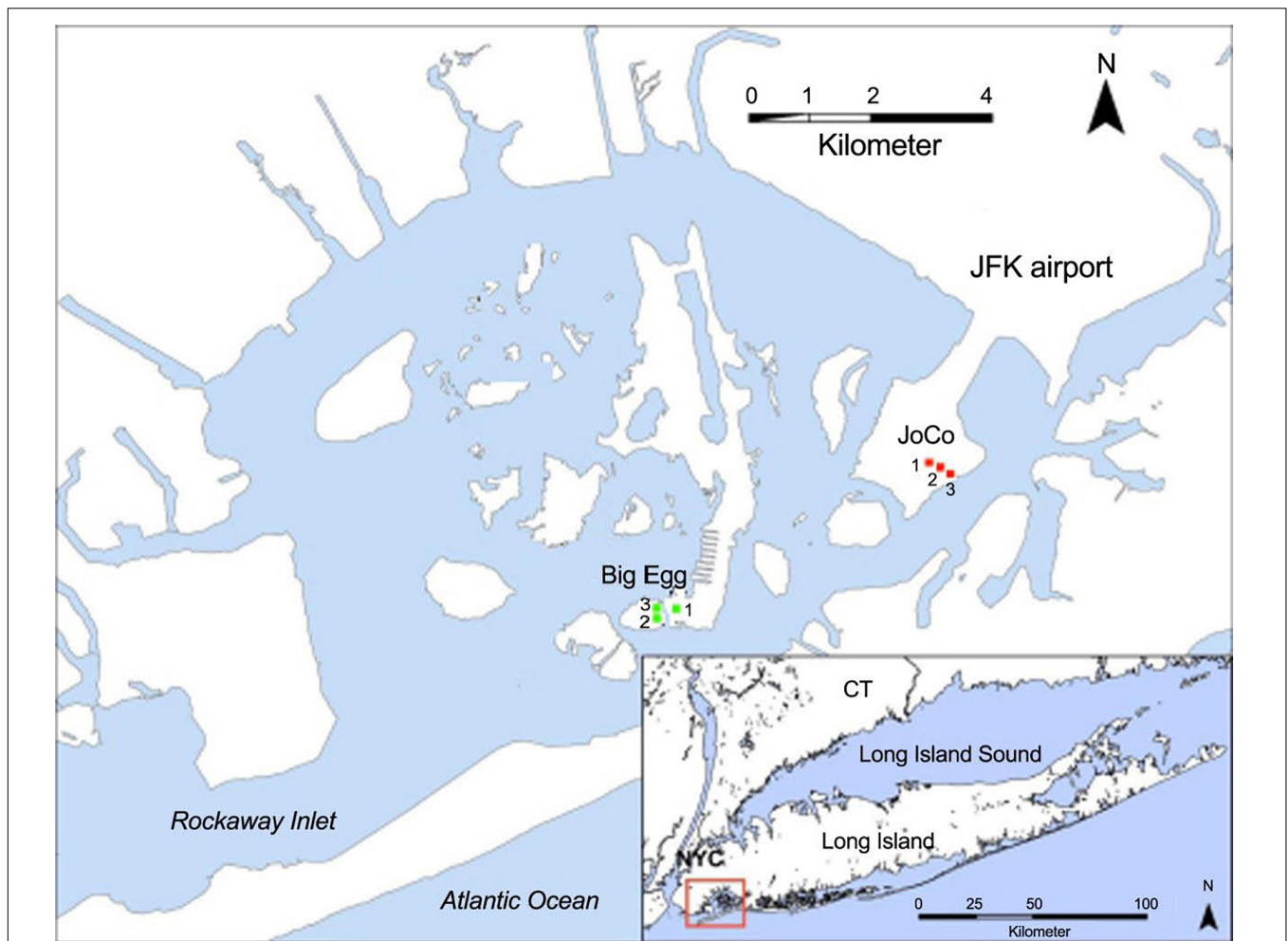


**FIGURE 1 |** Location of Jamaica Bay and the sampling sites at Big Egg (BE) and JoCo (JC). The GPS coordinates of sampling sites are BE1 (40.59604N, 73.82637W; restored in 2003), BE2 (40.59586N, 40.59586W), BE3 (40.59607N, 73.82812W), JC1 (40.61241N, 73.78779W), JC2 (40.61212N, 73.78724W), and JC3 (40.61173N, 73.78591W), respectively. Modified from Tamborski et al. (2017). Service Layer Credits: Source: Esri, DigitalGlobe, GeoEye, Earthstar Geographics, CNES/Airbus DS, USDA, USGS, AeroGRID, IGN, and the GIS User Community.

fall, but marsh plants grow well and it's still considered as a "healthy" marsh. On the other hand, marsh in the unrestored part of Big Egg seems to be worse, even the  $\text{H}_2\text{S}$  level is lower than JoCo. We hypothesize: (1) a complicated and time-dependent 3-D distribution pattern of low level dissolved  $\text{H}_2\text{S}$  and  $\text{Fe}^{2+}$  (cold-spots) around individual plant roots can be generated by oxygen transport/leakage from roots, and (2) the cold-spots/oxic layers formed around roots help marsh plants to survive in the high levels of  $\text{H}_2\text{S}$  by reducing sulfide absorption. Accordingly, we collected pore water samples with "sippers"– short tubes that are emplaced to various depths in the peat and through which pore water is drawn into an evacuated syringe, complemented this approach with chemical sensors that provide *in situ* high-resolution mapping linking the structure of marsh peat with spatial and temporal patterns of  $\text{H}_2\text{S}$  and  $\text{Fe}^{2+}$  concentrations, and collected marsh peat cores to study the distributions of Fe, S, N, C, and chromium reducible sulfur (CRS) in marsh peat solid phase. Our goal is to characterize the significant geochemical heterogeneities of Fe and S in marsh pore water and peat, seasonal

variation and the interactions of these solutes in marsh pore water, the characterization of elevated pore water levels of the phytotoxin  $\text{H}_2\text{S}$ , and the effects of the redox cycles of Fe and S on the solid phase reservoirs of these elements.

## MATERIALS AND METHODS

### Sample Sites

Jamaica Bay is a heavily urbanized estuary ( $\sim 80 \text{ km}^2$ ) located primarily between the New York City boroughs of Brooklyn and Queens, with a connection to the Atlantic Ocean through Rockaway Inlet (Figure 1). The Bay, consisting of over a dozen isolated marsh islands and a labyrinth of waterways, has been characterized as a eutrophic estuary with water salinity in the range of 20–26 PSU, temperature 1–26°C, and pH 6.8–9, respectively [USFWS (U.S. Fish and Wildlife Service), 1997]. Some of the marsh islands are natural, but many of them have been restored through engineering efforts. The dominant plant

species in the low salt marsh is saltmarsh cordgrass, *S. alterniflora*, and in the high salt marsh is salt meadow cordgrass, *Spartina patens*. These salt marshes provide critical ecological services, including habitat and food sources for wildlife, shoreline erosion control, and water column filtration, as well as serve as a buffer against storm tides and waves (New York City Department of Environmental Protection, 2007a,b; Marsooli et al., 2017). However, Jamaica Bay's salt marsh losses have been severe; about 60% of the Bay's salt marsh has converted into mudflats since 1951, with smaller islands losing up to 78% of their vegetation cover, due to a combination of factors including sediment load reduction, dredging, boat traffic, sea level rise, nutrient enrichment and H<sub>2</sub>S concentration increase (Rafferty et al., 2010; Campbell et al., 2017). The nutrient load of the Bay from sewage treatment plant effluent and combined sewer overflows is thought to be an important factor that may contribute to this high rate of marsh loss in recent years (Deegan et al., 2012).

Jamaica Bay has a mean semi-diurnal tidal range of approximately 1.5 m, the investigated marsh sites are all inundated during high tide. Two marsh sites were studied in the present work: one is a natural salt marsh, JoCo (JC), which is considered a "healthy" marsh, and the other is a partially restored salt marsh, Big Egg (BE). Three sampling sites were established in each marsh. One of the three sites at Big Egg (BE1) was previously restored by spraying sandy sediment from the adjacent channel onto the marsh surface as part of a restoration effort in 2003 (Frame et al., 2006), but the remaining two sites (BE2 and BE3) have not yet been restored. The two marshes are dominated by *S. alterniflora*, while JoCo has a mixture of marsh grasses that includes *Spartina patens*, a high marsh species. JoCo experienced a marsh loss of approximately 7% between 1974 and 1999, while losses at Big Egg were up to 38% (NYSDEC, 2006).

Pore water samples, solid marsh cores, and sensor deployment in JoCo were taken on October 10, 2014, May 1, 2015 and September 9, 2015 and April 22, 2016, respectively. In Big Egg sites, they were taken on October 8, 2014, April 13, 2015, September 25, 2015, and April 15, 2016, respectively.

## Discrete Pore Water Sampling and Measurements

Discrete pore water samples were taken using pore water "sippers" at depths of 5, 10, 15, and 25 cm in the marsh peat. The sippers are hollow acrylic rods that end in a small opening. Each sipper is connected to Tygon tubing which can be connected to a 50 ml plastic syringe. A valve connected to the Tygon tubing between the syringe and the sipper facilitates purging of the syringe. Pore water samples of ~50 ml were slowly drawn into the syringe through the sipper, and immediately filtered in the field through 0.45 μm filters. Aliquots for dissolved sulfide, nutrients, and trace elements were collected. The sulfide aliquots were fixed in the field by adding 0.5 ml of 0.05 M Zn(C<sub>2</sub>H<sub>3</sub>O<sub>2</sub>)<sub>2</sub>·2H<sub>2</sub>O to each sample, the Fe<sup>2+</sup> aliquots were stabilized by acidification. The concentrations of dissolved sulfide, nutrients (NH<sub>4</sub><sup>+</sup> and

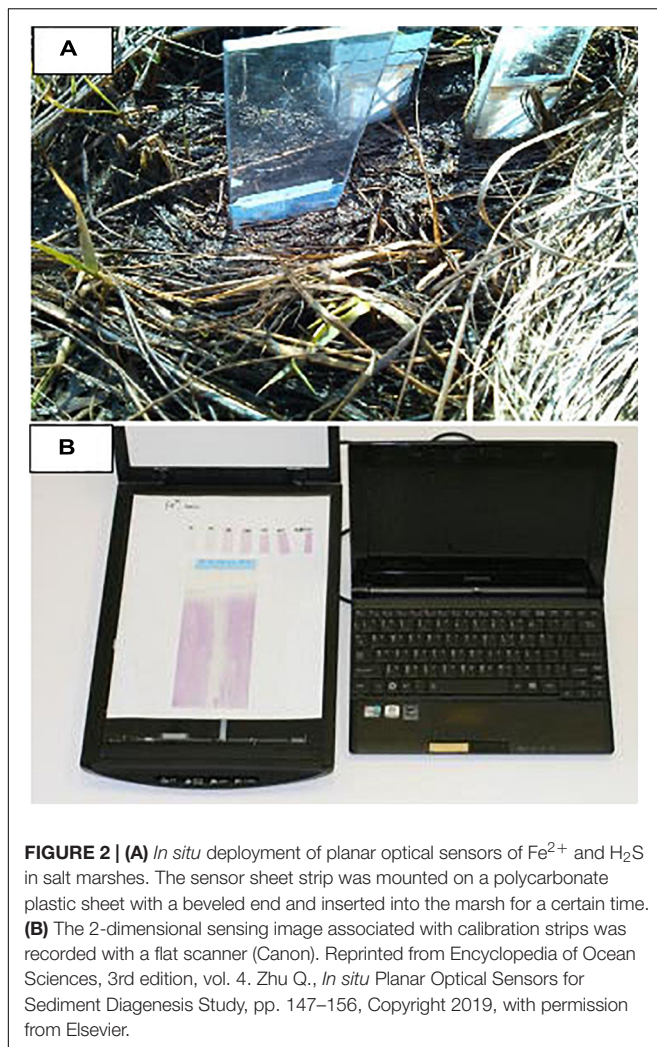
HPO<sub>4</sub><sup>2-</sup>) and dissolved Fe<sup>2+</sup> in these discrete pore water samples were subsequently measured in lab.

Total dissolved sulfide (as ΣH<sub>2</sub>S = [H<sub>2</sub>S] + [HS<sup>-</sup>] + [S<sup>2-</sup>]) and ammonium were measured using techniques described by Kolker (2005) and Cochran et al. (2013). Briefly, total sulfide was measured by spectrometric method (Cline, 1969; Reese et al., 2011) with relative standard deviation (RSD) < 5%. Ammonium and phosphate were measured using a Lachat Nutrient Autoanalyzer with RSD ± 5%, and dissolved Fe<sup>2+</sup> was determined by spectrometric method described by Stookey (1970). Pore water pH and E<sub>h</sub> (ORP; Oxidation-Reduction Potential) were measured in the field with a YSI 1009-1 09C multi-parameter probe that measured pH on the total H<sup>+</sup> scale and used a Pt electrode for E<sub>h</sub>. Salinity values were determined in the laboratory through measurement of chloride or with a refractometer.

## In situ Measurements of 2-D Pore Water H<sub>2</sub>S and Fe<sup>2+</sup> Using Optical Planar Sensors

2-D distributions of dissolved Fe<sup>2+</sup> in pore water were measured *in situ* by deploying optical planar Fe<sup>2+</sup> sensors in salt marsh. The irreversible planar sensor of dissolved Fe<sup>2+</sup> was fabricated with ferrizone as the optical indicator that was immobilized in polyurethane hydrogel (D4) membrane, modified from our previous publication (Zhu and Aller, 2012). The blank Fe<sup>2+</sup> sensor film was colorless and transparent, and it rapidly converted to a violet-red color with maximum absorption wavelength at 562 nm after the sensor film was exposed to dissolved Fe<sup>2+</sup> solution. The sensor response range depends on the sensor deployment time in Fe<sup>2+</sup> solution, and the sensor showed a good linear response in the range of 0–200 μmol/L of Fe<sup>2+</sup> with the limit of detection of 5 μmol/L when a 10 min deployment time was applied. A short sensor deployment time was used when Fe<sup>2+</sup> concentration was higher than 200 μmol/L, and the sensor could respond to dissolved Fe<sup>2+</sup> as high as 1 mmol/L when it was deployed in the sample for 1 min. In this work, 1–10 min Fe<sup>2+</sup> sensor deployment time in salt marsh was used, depending on the Fe<sup>2+</sup> concentration in the marsh pore water.

The sensor film sheet (14 cm × 20 cm) was cut into five sensor film stripes with dimension of 2.8 cm × 20 cm, four strips were used for *in situ* deployment and one for calibration. The sensor film strip was mounted on a 5 cm × 40 cm × 1 cm (width × length × thickness) polycarbonate plastic sheet with a beveled end. *In situ* measurements were performed at low tide by inserting/punching the plastic sheet with attached sensor strip vertically into the salt marsh peat (Figure 2) and allowing it to react with dissolved Fe<sup>2+</sup> in pore water for 1–10 min. After the reaction, the sensor film was pulled out of the marsh and rinsed with seawater. The color-developed Fe<sup>2+</sup> sensing film was then wrapped with a paper towel and brought back to the laboratory for imaging. *In situ* measurements were duplicated at each marsh sample site. After return to the laboratory, the sensor films were calibrated with identical response time by using Fe<sup>2+</sup> standards prepared in seawater which was collected from the



same sample site. The colored  $\text{Fe}^{2+}$  sensor strips were imaged by a flat scanner (Canon), and all color images were analyzed with Maxim DL image processing software version 2.0X (Diffraction Limited) and Image-Pro plus version 4.1 for Windows (Media Cybernetics). The isolated green bands of the color images were used to calculate the absorbance within individual pixels. *In situ* measurements of 2-D  $\text{Fe}^{2+}$  distributions in pore water were conducted at October 2014, April 2015, and September 2015.

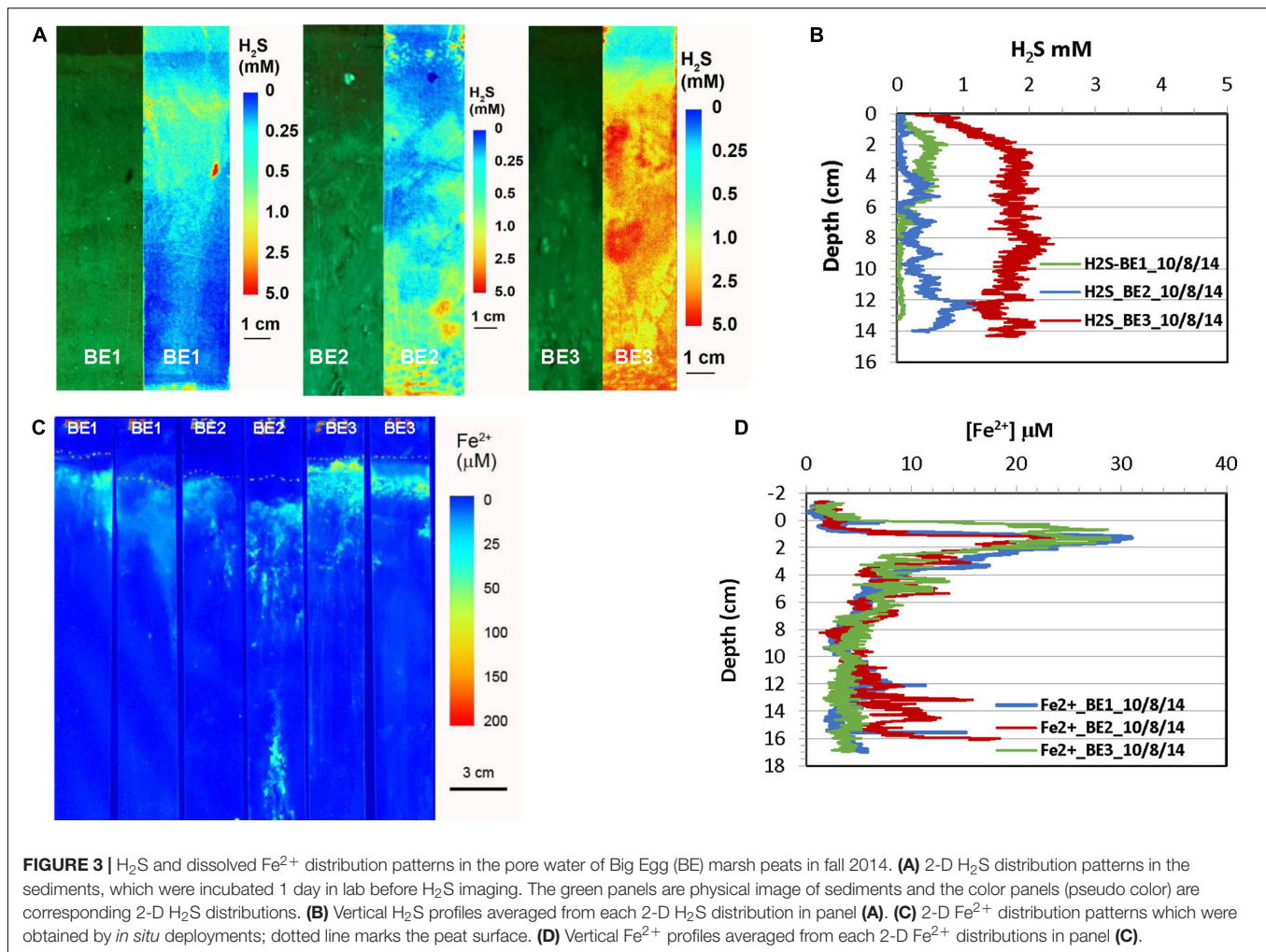
2-D distributions of dissolved  $\text{H}_2\text{S}$  in salt marshes were measured by two different optical planar  $\text{H}_2\text{S}$  sensors. The 2-D  $\text{H}_2\text{S}$  distributions in the October 2014 samples were measured by a fluorescence planar sensor in box cores which were collected from each site and incubated/re-equilibrated with seawater (collected from the same site) in the laboratory for 24 h at room temperature ( $22^\circ\text{C}$ ) with constant aeration of overlying water. The fluorescence  $\text{H}_2\text{S}$  planar sensor sheet was prepared by non-covalently immobilizing  $\text{H}_2\text{S}$  fluorescence indicator pyronin in an ethyl cellulose polymer membrane on a transparent polyester sheet, and coating with a layer of gas permeable silicone (Zhu and Aller, 2013). The fluorescence sensor responded well to dissolved  $\text{H}_2\text{S}$  in the range of non-detectable to  $3.15 \text{ mmol/L}$  with detection limit  $40 \mu\text{mol/L}$  dissolved  $\text{H}_2\text{S}$ . The sensor response time was

about 60 s, and it was very suitable for  $\text{H}_2\text{S}$  quantification in highly sulfidic salt marshes. However, it was only a moderately reversible fluorescence sensor, losing its response after 5–6 measurement cycles (Zhu and Aller, 2013). The sensor film was cut into the strips of  $3 \text{ cm} \times 15 \text{ cm}$  for the following 2-D measurement: an  $\text{H}_2\text{S}$  sensor strip was installed on the inside of the front face of the box corer and sensing membrane contacted to the marsh sediment. The bottom of the box core was tightly sealed. After 24 h incubation, the fluorescence image of the  $\text{H}_2\text{S}$  sensor strip was taken at  $577 \text{ nm} (\pm 10 \text{ nm})$  with excitation wavelength at  $554 \text{ nm}$  by using our home-made imaging system (Zhu and Aller, 2013). Image analysis and data calculations were performed with Maxim DL image processing software version 2.0X (Diffraction Limited) and Image-Pro plus version 4.1 for Windows (Media Cybernetics). Images were split into blue, green and red bands and the red band was used to calculate the intensities of individual pixels.

2-D  $\text{H}_2\text{S}$  distributions in other seasons, April 2015 (spring) and September 2015 (late summer), were obtained by *in situ* deployments using an irreversible  $\text{H}_2\text{S}$  colorimetric planar sensor that was prepared from diphenylcarbazone- $\text{Zn}^{2+}$  complex in polyurethane hydrogel (D4) on a transparent polyester sheet, covered by a gas permeable silicone membrane to eliminate possible interfering hydrated ions. The blank sensor film showed a dark purple color with a maximum absorbance at  $530 \text{ nm}$ , and the sensor absorbance was inversely correlated with dissolved  $\text{H}_2\text{S}$  concentration in the range of  $5\text{--}4,000 \mu\text{mol/L}$  (Yin et al., 2017). A  $3.5 \text{ cm} \times 20 \text{ cm}$   $\text{H}_2\text{S}$  sensor film was mounted on one side of a  $5 \text{ cm} \times 40 \text{ cm} \times 1 \text{ cm}$  (width  $\times$  length  $\times$  thickness) polycarbonate plastic sheet with a beveled end, and the deployment method was the same as 2-D  $\text{Fe}^{2+}$  *in situ* measurement as described above. Response time of the  $\text{H}_2\text{S}$  sensor in marsh was 1–10 min (depend on the  $\text{H}_2\text{S}$  concentration in the marsh). After the reaction, the sensor film was pulled out of the sediment and rinsed with seawater. The color-changed sensing film was scanned within 20 min in the field by using a flat scanner (Canon). After return to the lab, the  $\text{H}_2\text{S}$  sensor responses were calibrated for identical response times by using  $\text{H}_2\text{S}$  standard solutions prepared from sodium sulfide in  $\text{pH} < 4$  solutions. All color images, including sample sensing images, were analyzed with Maxim DL image processing software version 2.0X (Diffraction Limited) and Image-Pro plus version 4.1 for Windows (Media Cybernetics). The isolated green bands of the color images were used to calculate the absorbance within individual pixels.

## Solid Phase Geochemistry

Cores for solid phase geochemistry (sulfur and iron) were taken by carefully inserting an aluminum tube (i.d., 7 cm) into the marsh peat. After the tube was positioned on the marsh surface, vertical cuts were made around the perimeter to minimize compaction as the core was inserted. Immediately after return to the laboratory, the cores were frozen. They were later defrosted only enough to permit the sediment to be extruded and then were sectioned into 1–2 cm intervals. The JoCo sediment cores had more peat and roots whereas the Big Egg sediment cores had fewer large roots and more mud. Small aliquots of sediment were removed from each section for solid phase geochemistry and the



remainder was weighed, dried, weighed again to determine water content and then ground to a powder. Solid phase reactive iron was measured by leaching ~50 mg of dried sediment in 1 N HCl for 24 h at room temperature. Total Fe in the leach solution was measured colorimetrically using the ferrozine method (Stokey, 1970). Sulfur was measured in two pools—chromium reducible sulfides (CRS, dominantly pyrite, and FeS<sub>2</sub>) and total sulfur, as described in Kolker (2005) and Cochran et al. (2013).

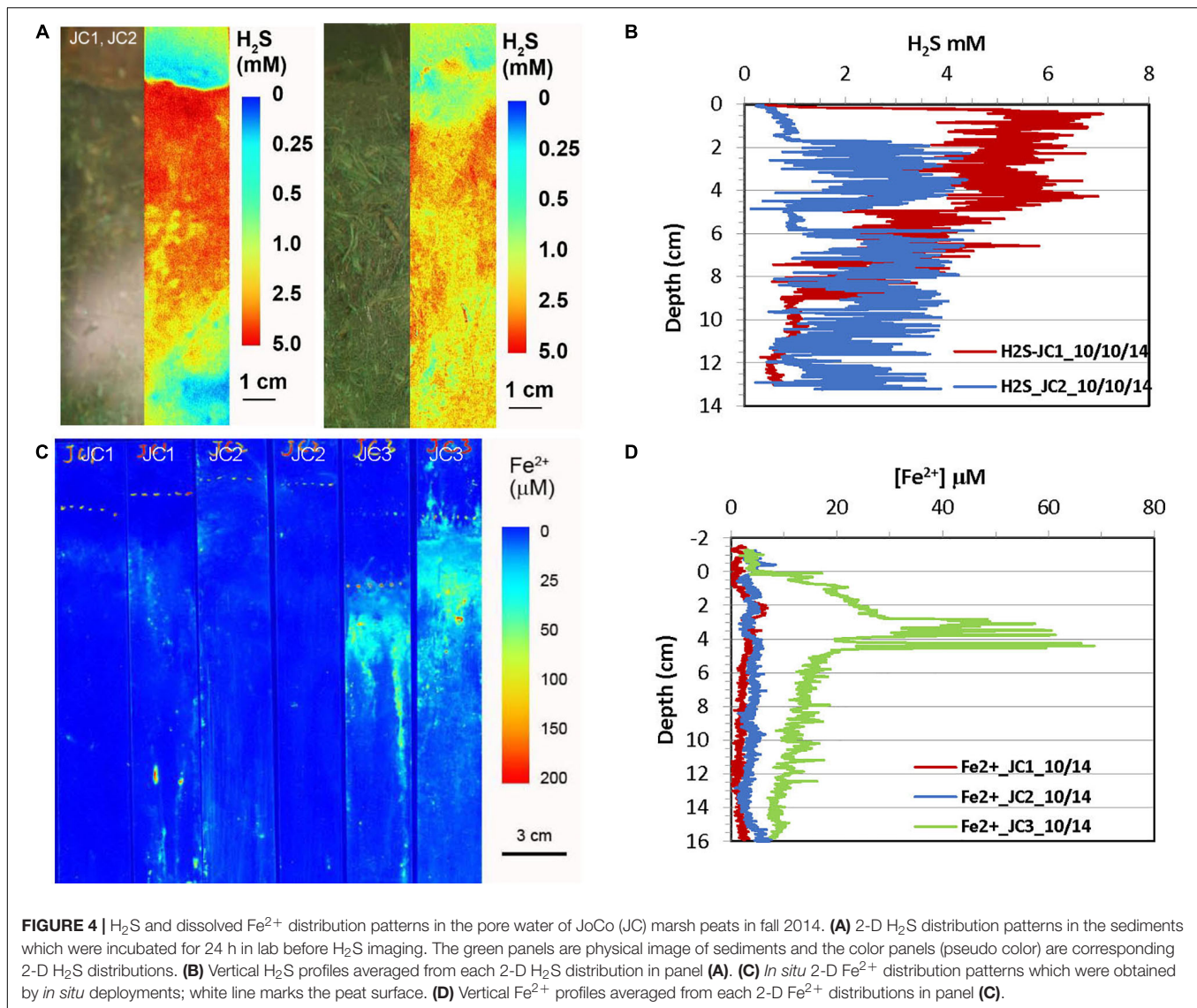
## RESULTS

The high resolution 2-D Fe<sup>2+</sup> and 2-D H<sub>2</sub>S distribution patterns revealed by optical sensors in the six sampling sites in Big Egg (BE) and JoCo (JC) are shown in **Figures 3–8**. Vertical profiles of dissolved H<sub>2</sub>S and Fe<sup>2+</sup> at each site were calculated by averaging the data across each horizontal pixel layer.

The results of H<sub>2</sub>S and Fe<sup>2+</sup> distributions in the early fall sampling (October 2014) obtained by optical sensors are given in **Figures 3, 4**. The green panels in **Figures 3A, 4A** are visible images of the side views of marsh cores from Big Egg and JoCo, respectively. The root interweaving patterns can be clearly

seen and are directly associated with the 2-D H<sub>2</sub>S distribution patterns. The H<sub>2</sub>S in all sampling sites showed a gradient in the top 10 cm depth. H<sub>2</sub>S level in the surficial sediment of BE1 increased with depth and formed a maximum concentration band from 2 to 5 cm depth, with H<sub>2</sub>S 0.5 mM, then sharply decreased to almost 0 below 6 cm. H<sub>2</sub>S in BE2 also increased with depth but reached a maximum concentration ~1 mM H<sub>2</sub>S below 12 cm. Higher H<sub>2</sub>S concentration was observed in BE3 where H<sub>2</sub>S sharply increase from 0 to 2 mM in top 2 cm marsh and then reached maximum H<sub>2</sub>S concentration below this depth. The 2-D H<sub>2</sub>S distribution patterns in the BE sites showed significant lateral and vertical heterogeneities even though site BE2 was very close to BE3. Many “hot spots” of H<sub>2</sub>S in the marsh were also elevated. However, the dissolved Fe<sup>2+</sup> in the three sites BE1–3 showed a similar distribution pattern (**Figures 3C,D**). Fe<sup>2+</sup> concentration sharply increased just below the water-sediment interface and reached Fe<sup>2+</sup> maximum zone at 1–2 cm deep and then quickly dropped to non-detectable level. The maximum Fe<sup>2+</sup> concretions in all BE sites were between comparable, with values of 20–30 μM Fe<sup>2+</sup> in pore water (**Figure 3D**).

**Figure 4** shows the H<sub>2</sub>S and Fe<sup>2+</sup> distributions in JoCo in the early fall season. Compared with their distributions in Big

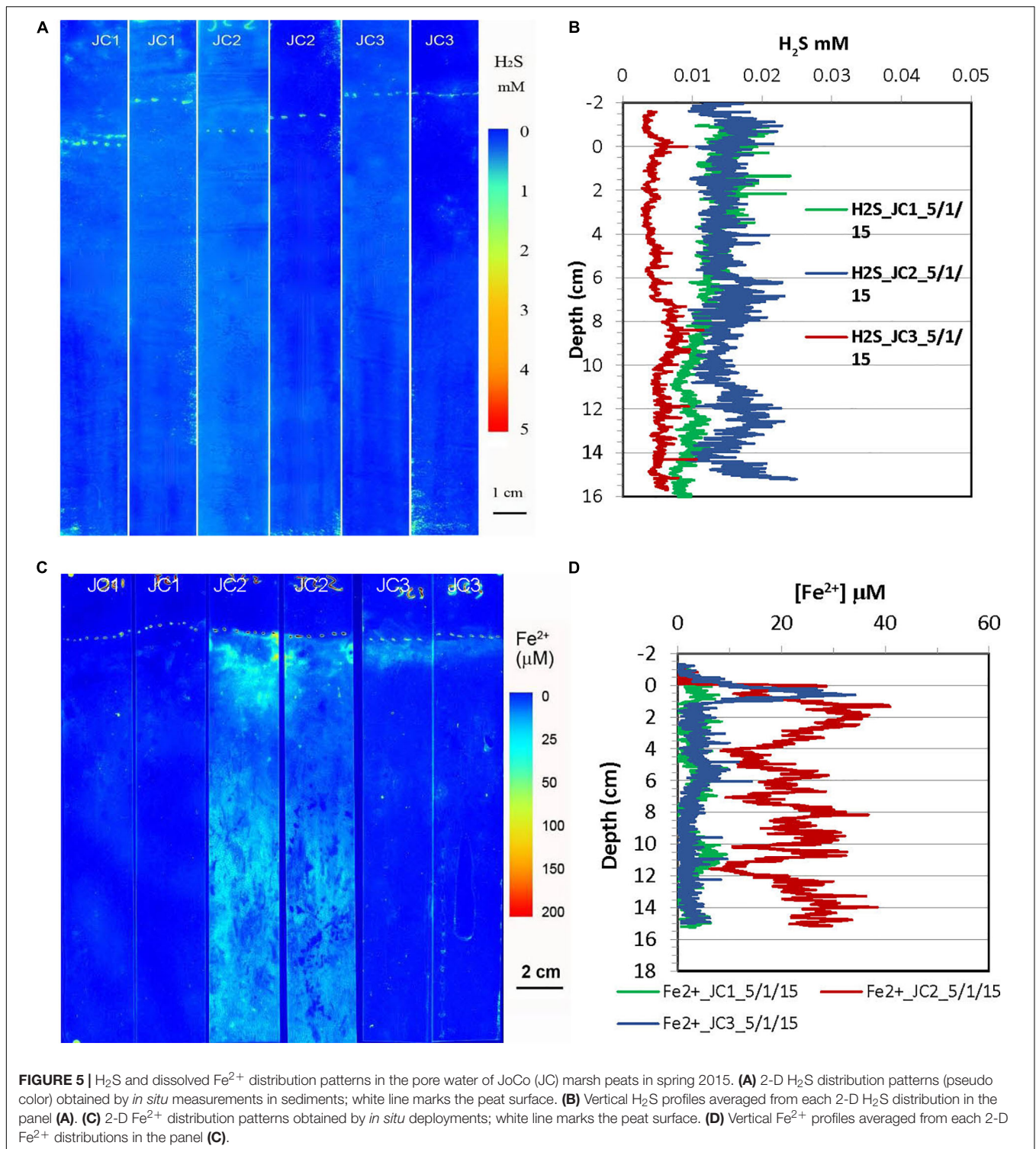


Egg,  $\text{H}_2\text{S}$  concentrations in JoCo, 3–6 mM, are much higher than those in Big Egg.  $\text{H}_2\text{S}$  concentration in JC1 immediately reached a maximum of 6 mM just below the sediment surface and gradually decreased to 1 mM at 12 cm (**Figures 4A,B**). Accordingly, no  $\text{Fe}^{2+}$  was found in JC1 and JC2 sites except some  $\text{Fe}^{2+}$  hot spots due to the high and constant level of  $\text{H}_2\text{S}$ . The 2-D  $\text{Fe}^{2+}$  distribution pattern in JC3 is similar to that in the BE sites, but reached the maximum zone at 4 cm with  $\text{Fe}^{2+}$  concentration around 40  $\mu\text{M}$ . It should be emphasized that the 2-D  $\text{H}_2\text{S}$  distributions in the fall 2014 season were measured in the laboratory with a box core incubation for 24 h at room temperature, using a fluorescence  $\text{H}_2\text{S}$  sensor (see section “Materials and Methods,” Zhu and Aller, 2013). 2-D  $\text{H}_2\text{S}$  distributions in all other seasons were measured *in situ* with optical sensor sheets, as done for the 2-D  $\text{Fe}^{2+}$  distribution patterns.

2-D  $\text{H}_2\text{S}$  and  $\text{Fe}^{2+}$  distributions in the spring season at the site of JoCo and Big Egg were measured *in situ* on 05/01/2015

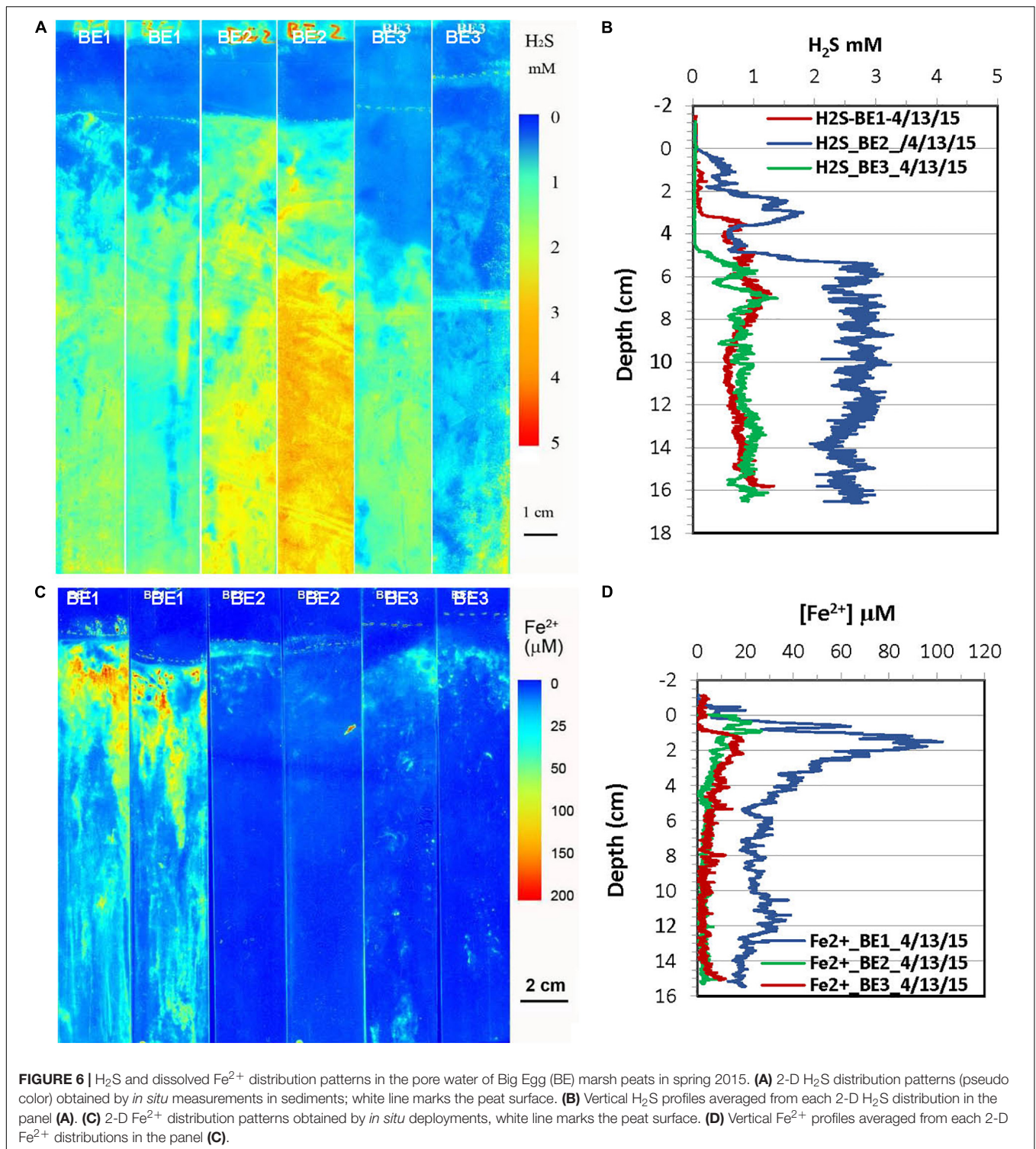
and 04/13/2015 (**Figures 5, 6**), respectively. The concentrations of  $\text{H}_2\text{S}$  were generally <20  $\mu\text{M}$  or non-detectable in the top 15 cm of marsh in JoCo (**Figure 5**), however, higher levels of  $\text{H}_2\text{S}$  (1–3 mM) were found at the sites of BE1-3 associated with root distribution patterns (**Figure 6**). Dissolved  $\text{Fe}^{2+}$  concentrations were non-detectable at JC1 in the top 15 cm, meanwhile dissolved  $\text{Fe}^{2+}$  was high (20–30  $\mu\text{M}$ ) in a very thin 0.5–2 cm layer at JC2, BE2, and BE3. Relatively higher  $\text{Fe}^{2+}$  levels were observed at JC2 and BE1, particularly at BE1, where dissolved  $\text{Fe}^{2+}$  was present from the sediment surface to 15 cm deep ( $\text{Fe}^{2+}$  was not measured deeper than 15 cm in any sampling) with a maximum concentration of 100  $\mu\text{M}$  at 2 cm. The results showed that both dissolved  $\text{H}_2\text{S}$  and  $\text{Fe}^{2+}$  concentrations in Big Egg site were higher than those at JoCo in the spring season.

2-D distribution patterns of  $\text{H}_2\text{S}$  and  $\text{Fe}^{2+}$  in marsh pore water were mapped in a late summer sampling in September 2015, and the results from are summarized in **Figures 7, 8**, respectively.  $\text{H}_2\text{S}$  concentrations were almost non-detectable in



the top 2 cm of marsh but started to significantly increase below this depth and reached maximum concentrations of 2–3 mM at about 10 cm at the JC1 and JC2 sites.  $\text{H}_2\text{S}$  concentrations at sites of JC3, BE1, and BE2 were in the range of 1–1.5 mM below 8 cm which was smaller than that in JC1 and JC2, and no  $\text{H}_2\text{S}$  was observed in the top 8 cm. At BE3,  $\text{H}_2\text{S}$  was immediately

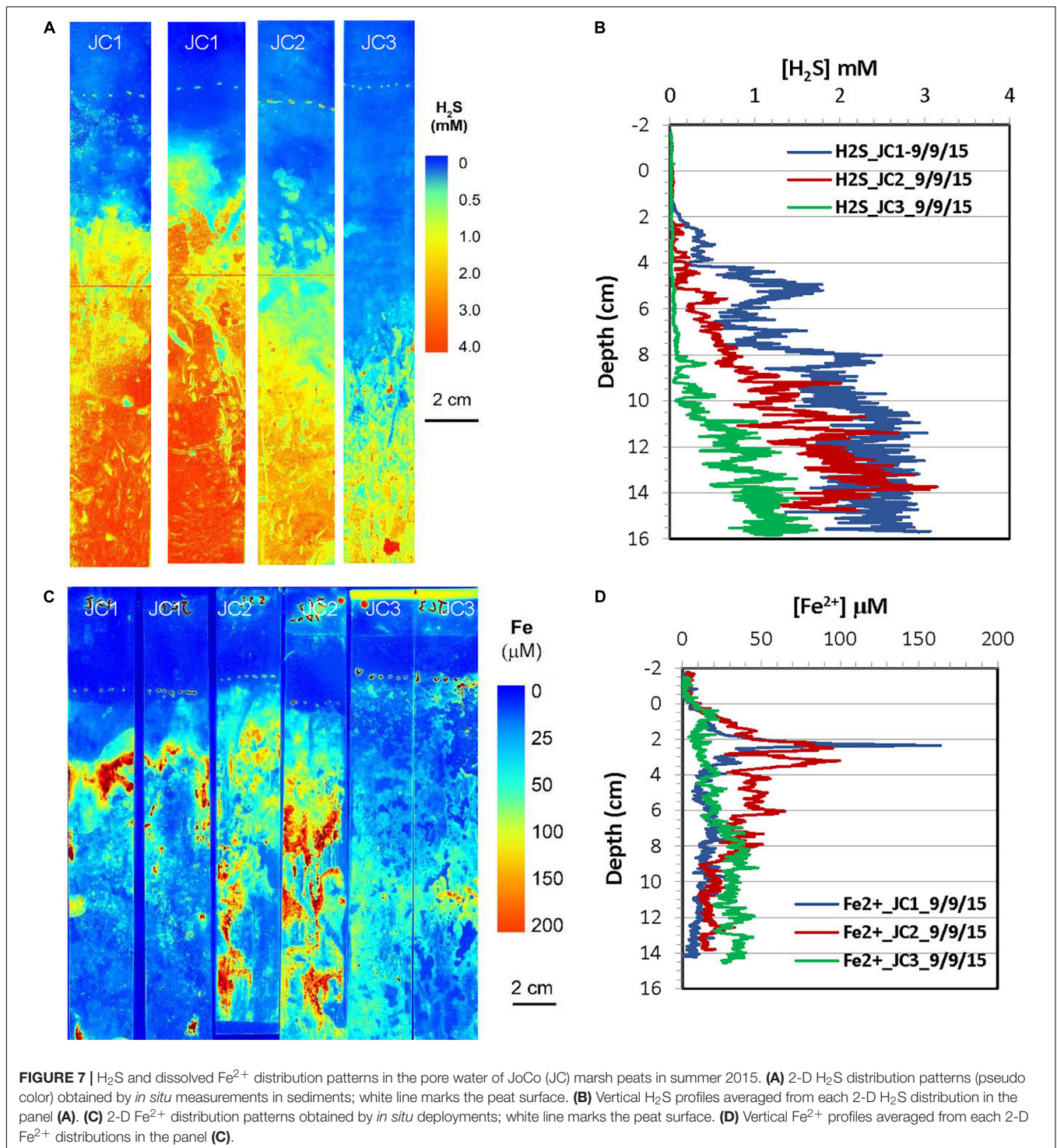
elevated under marsh surface and increased to > 2 mM  $\text{H}_2\text{S}$  below 4 cm depth. Similarly to the 2-D  $\text{H}_2\text{S}$  distributions obtained in the lab (**Figures 3A, 4A**), complicated and heterogeneous  $\text{H}_2\text{S}$  distributions in the marsh can be seen associated with rhizospheres structures (**Figures 7A, 8A**). 2-D  $\text{Fe}^{2+}$  vertical distributions in all JoCo sites in summer showed very large



variations and many “hot spots” and “cold spots” from the marsh surface down to 14 cm depth.  $\text{Fe}^{2+}$  concentrations at the hot spots may have reached as high as  $>200 \mu\text{M}$  (Figure 7C), but may have sharply dropped to non-detectable levels in cold spots. In general, the average  $\text{Fe}^{2+}$  concentrations in JoCo were smaller than those at the Big Egg sites, where  $\text{Fe}^{2+}$  showed a

maximum zone from 0 to 4 cm, with concentrations of 50–200  $\mu\text{M}$ , and sharp decreases to  $<50 \mu\text{M}$  or non-detectable below 4 cm (Figure 8C).

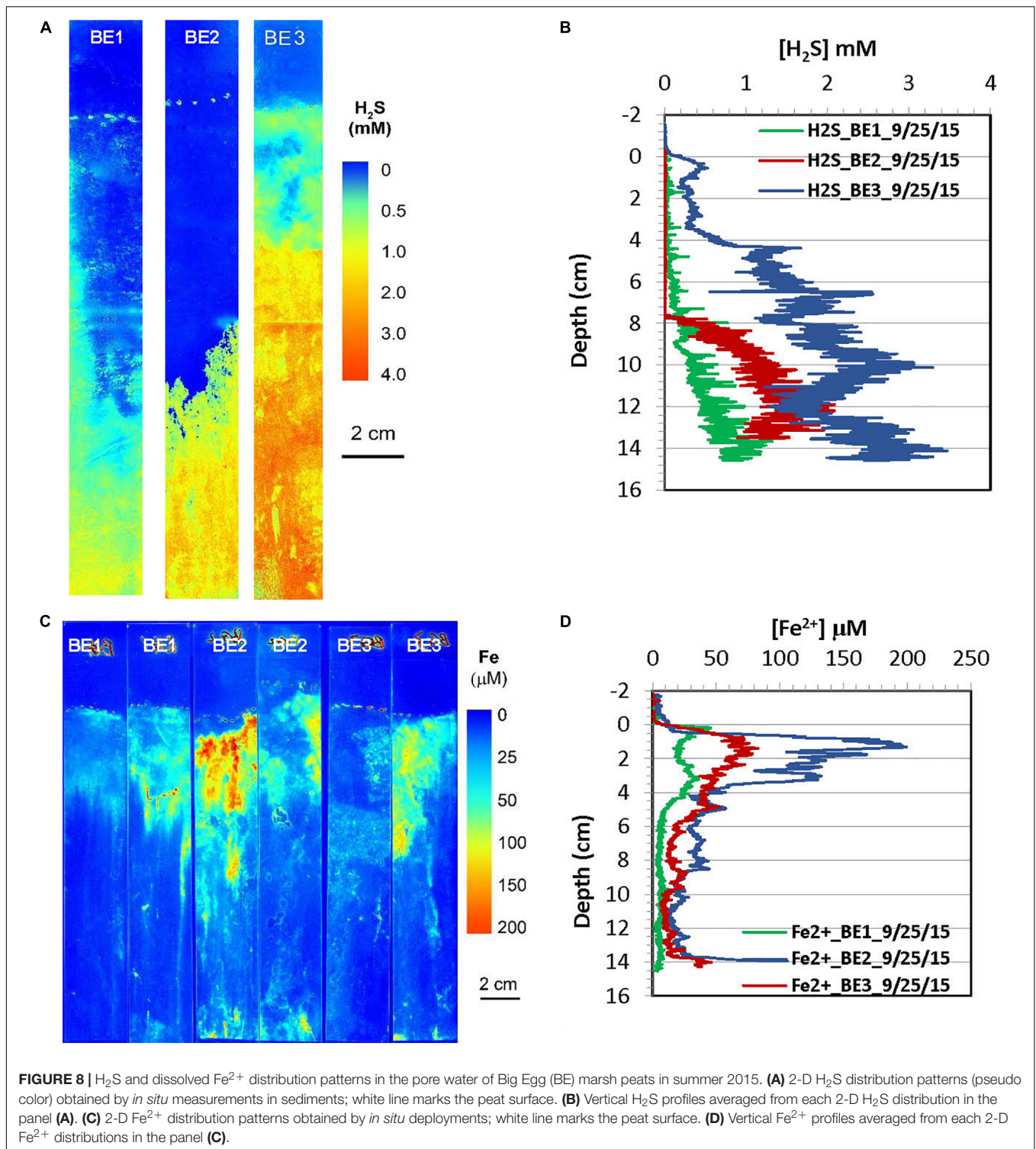
The pH, redox potentials ( $E_h$ ) and salinity of the discrete pore water samples collected at 5, 10, 15, and 25 cm depth at the marsh sites during different seasons are summarized in Table 1. The pH



values of all sites and seasons were mostly  $<7$ , and the vertical pH data showed slight increases with depth below 5 cm. No obvious pH seasonal variation was observed at all depths. However, the pH at JoCo was likely lower than pH of Big Egg at the same depth in the same season.

Redox potential ( $E_h$ ) obtained from each marsh site below 5 cm was negative. It decreased with depth at most sites and also

showed a significant seasonal and spatial variation for both Big Egg and JoCo marsh sites. At JoCo, the  $E_h$  of summer and fall ranged from  $\sim -200$  to  $\sim -350$  mV, and it increased to  $-40$   $\sim -170$  mV in spring. The  $E_h$  values at Big Egg were in the range of  $-12$  to about  $-380$  mV in summer and fall, but showed high spatial and temporal variance. In the spring season, the  $E_h$  values of Big Egg were in the range of  $-200$   $\sim -250$  mV at all



depth, but this was consistent with the high  $\text{H}_2\text{S}$  values found in spring in this marsh (Figures 6A,B). The salinities of all sampling sites did not show obvious changes either with depth or season, ranging from 27 to 30.

The concentrations of  $\text{Fe}^{2+}$ , total hydrogen sulfide ( $\Sigma\text{H}_2\text{S}$ ), phosphate and ammonium in pore water were also determined

by traditional methods *via* “sipper” sample collection method at discrete depths of 5, 10, 15, and 25 cm. The results are summarized in Table 2.  $\text{Fe}^{2+}$  in pore water of JoCo and Big Egg were generally very low ( $<10 \mu\text{M}$ ) and no obvious changes with depth except the spring data of JC2 which increased from 77 to 141  $\mu\text{M}$  from 5 to 16 cm. The relative high  $\text{Fe}^{2+}$  concentration of

**TABLE 1** | Pore water pH, redox potential and salinity data obtained *in situ* in Big Egg and JoCo marshes, Jamaica Bay, NY.

Marsh Site	Depth (cm)	pH			Redox potential $E_h$ (mV)			Salinity (PSU)		
		Fall '14	Spring '15	Summer '15	Fall '14	Spring '15	Summer '15	Fall '14	Spring '15	Summer '15
<b>JoCo</b>		<b>10/10/14</b>	<b>5/1/15</b>	<b>9/9/15</b>	<b>10/10/14</b>	<b>5/1/15</b>	<b>9/9/15</b>	<b>10/10/14</b>	<b>5/1/15</b>	<b>9/9/15</b>
JC1	5	6.45	4.88	6.2	-230	-41	-325	28	32	ND
	10	6.41	6.08	6.15	-273	-60	-325	29	27	ND
	15	6.50	6.04	6.35	-270	-90	-350	29	28	ND
	25	6.55	6.25	6.23	-290	-210	-350	29	27	ND
JC2	5	6.30	5.40	6.82	-185	-39	-198	28	28	ND
	10	6.55	5.70	6.15	-220	-113	-277	28	26	ND
	15	6.35	5.62	6.13	-230	-98	-307	28	25	ND
	25	6.60	6.30	5.77	-250	-160	-321	28	24	ND
JC3	5	6.13	5.87	6.64	-220	-86	-234	29	35	ND
	10	6.42	6.04	6.06	-270	-106	-247	30	31	ND
	15	6.53	6.67	6.12	-275	-128	-320	32	27	ND
	25	6.64	6.32	5.95	-285	-164	-235	32	28	ND
<b>Big Egg</b>		<b>10/8/14</b>	<b>4/13/15</b>	<b>9/25/15</b>	<b>10/8/14</b>	<b>4/13/15</b>	<b>9/25/15</b>	<b>10/8/14</b>	<b>4/13/15</b>	<b>9/25/15</b>
BE1	5	6.12	7.01	IV	-125	-190	IV	27	28	ND
	10	5.74	7.09	6.79	-75	-233	-345	27	27	ND
	15	6.36	7.12	IV	-190	-186	IV	27	28	ND
	25	6.45	6.84	6.85	-133	-186	-367	27	28	ND
BE2	5	6.70	NS	7.15	-27	NS	-371	28	NS	ND
	10	7.10	7.08	7.02	-12	-217	-374	28	29	ND
	15	IV	6.52	IV	IV	-230	IV	30	29	ND
	25	6.50	6.65	6.67	-240	-195	-383	29	29	ND
BE3	5	6.00	NS	NS	-130	NS	NS	28	NS	NS
	10	6.46	6.88	NS	-200	-250	NS	28	30	NS
	15	6.50	7.26	NS	-150	-187	NS	29	30	NS
	25	6.34	7.09	NS	-230	-186	NS	29	30	NS

ND, not determined; IV, insufficient volume for electrode; NS, no sample.

JC2 in spring was also observed by the optical sensor (Figure 5C), but no spatial and seasonal variances of  $Fe^{2+}$  concentrations were observed by the traditional lab methods.  $\Sigma H_2S$  measured in the fall and summer seasons was typically higher than in the spring season, and the average  $\Sigma H_2S$  concentrations at the JoCo sites were higher than those at Big Egg. However, the BE sites showed much higher  $\Sigma H_2S$  than JC in the spring season, which was consistent with the dissolved  $H_2S$  level obtained by *in situ* sensing (Figures 5A, 6A). Ammonium concentrations also varied with season and location in Jamaica Bay. The  $NH_4^+$  concentrations at sites in BE were as high as 100–900  $\mu M$  in spring and summer, but decreased to <158  $\mu M$  in fall. The  $NH_4^+$  concentrations of JC in spring and summer were much lower than those of BE, but they were higher than BE in fall. Similar to ammonium, phosphate also showed relative higher concentrations at the site of BE, and the phosphate concentration sequence at different seasons were summer > spring > fall in both BE and JC sites.

The solid phase organic carbon, total sulfur (S), CRS acid leaching Fe and degree of pyritization (DOP) at different sites and seasons are summarized in Table 3. Total sulfur concentrations in JC were slightly higher in fall season, but its distribution at BE2

was different from other sites and higher sulfur was observed in spring at BE2. CRS showed higher concentrations at each depth in the spring than that in summer. It was typically increased with depth but a decreasing pattern was found at site BE2. The distribution patterns of acid-leachable iron in JC and BE were also different— all three JoCo sites showed higher solid phase Fe in summer than in spring, but in contrast, Big Egg marsh had much higher solid phase Fe in spring than summer. CRS and acid leachable Fe in the fall season were not analyzed.

## DISCUSSION

### Heterogeneities of $Fe^{2+}$ and $H_2S$ Distributions in Salt Marsh Pore Water

Salt marshes are sites of intense biogeochemical reactions involving anoxic organic matter remineralization, which typically result in dramatic changes in the concentration of  $H^+$ ,  $Fe^{2+}$ ,  $H_2S$ , and other pore water species in the upper layer of marsh sediments (Morse et al., 1987; Canfield et al., 1992; Brendel and Luther, 1995; Bull and Taillefert, 2001; Zhu and Aller, 2013; Yin et al., 2017; Koop-Jakobsen et al., 2018).

**TABLE 2** | Pore water solute data obtained from Big Egg and JoCo marshes, Jamaica Bay, NY.

Marsh Site	Depth (cm)	NH <sub>4</sub> <sup>+</sup> (μM)			HPO <sub>4</sub> <sup>3-</sup> (μM)			ΣH <sub>2</sub> S (μM)			Fe <sup>2+</sup> (μM)		
		Fall '14	Spring '15	Summer '15	Fall '14	Spring '15	Summer '15	Fall '14	Spring '15	Summer '15	Fall '14	Spring '15	Summer '15
JC1	5	2.0	57	4.9	0.2	3.6	14	2,876	4.5	2,314	3	8	5
	10	23	157	41	0.2	7.9	20	6,095	17	4,301	3	3	NS
	15	28	193	134	0.2	8.7	20	5,587	43	4,658	7	6	NS
	25	77	224	96	0.3	9.2	24	6,697	660	4,275	2	7	NS
JC2	5	36	1.6	0.0	0.4	0.0	4.3	846	5.4	NS	2	77	15
	10	71	2.6	0.0	0.5	0.0	1.0	1,594	4.5	133	3	96	15
	15	2.6	7.3	0.0	0.3	0.0	1.1	1,973	133	588	3	141	NS
	25	198	41	2.0	1.0	7.2	4.7	3,487	343	1,800	4	11	NS
JC3	5	10	26	31	0.2	1.1	11	3,470	2.1	282	4	6	15
	10	71	181	35	0.5	4.5	11	5,406	4.9	480	6	4	15
	15	102	291	11	0.1	6.4	22	9,416	24	4,056	4	3	NS
	25	170	248	23	0.4	7	22	8,539	390	2,891	20	6	NS
BE1	5	14	240	111	0.1	11	90	1,234	272	1,200	5	2	11
	10	4.2	340	207	0.0	40	161	252	882	3,015	5	2	5
	15	59	265	344	0.4	28	44	17	413	1,370	6	4	0
	25	1.0	245	445	0.1	20	91	85	509	5,381	6	3	1
BE2	5	18	882	589	0.2	85	115	17	2,476	2,962	2	3	0
	10	28	336	752	0.2	26	130	9	926	4,022	3	3	2
	15	NS	160	522	NS	24	111	4,965	2,576	3,178	4	4	5
	25	158	73	637	0.9	11	100	4,436	1,431	5,491	3	2	2
BE3	5	5.8	NS	582	0.3	NS	164	273	1,846	2,143	4	NS	3
	10	4.8	610	759	0.4	72	212	840	226	4,164	4	1	4
	15	6.5	207	NS	2.1	13	NS	2,116	368	3,916	3	2	NS
	25	14	238	762	1.0	15	85	2,366	NS	6,722	3	1	6

NS, no sample.

Compositional changes of Fe<sup>2+</sup> and H<sub>2</sub>S with depth in sediment pore water are usually assumed to occur in an overall average vertical progression. Significant heterogeneity and complex three dimensional reaction patterns over mm to cm scales can result, however, from bioturbation activity (Zhu and Aller, 2013; Yin et al., 2017). In salt marshes, the growth of wetland plants and oxygen transport through the aerenchyma lacunae of plants from aboveground sources to rhizosphere can also create a complicated thin layer of aerobic environment around roots through the radial oxygen loss (ROL) from roots (Armstrong, 1979; Howes and Teal, 1994; Colmer, 2003; Han et al., 2016; Koop-Jakobsen et al., 2018). Most of the selected study sites in Jamaica Bay are dominated by saltmarsh cordgrass *S. alterniflora*, in which the roots extensively intergrow into a dense network over at least the top 30 cm of the peat. Thus, it is expected that the 2-D distribution patterns of Fe<sup>2+</sup> and H<sub>2</sub>S in marsh peat are influenced by the plant root growth patterns. We hypothesize that the oxygen transport through plant rhizosphere and the radial oxygen loss can generate a time-dependent 3-D distribution pattern of low level dissolved H<sub>2</sub>S and Fe<sup>2+</sup> (cold-spots) associated with individual plant roots in marsh peat.

In order to test this hypothesis and study Fe<sup>2+</sup> and H<sub>2</sub>S distributions and the associated biogeochemical processes in marsh peat with a high density of living plants, box cores made of clear acrylic plastic were collected from each site in

October 2014 and the H<sub>2</sub>S sensor deployments were conducted in the laboratory so that the plant root features and sensor foil deployment position can be directly seen from side of the core. The 2-D H<sub>2</sub>S distribution measured by a reversible H<sub>2</sub>S fluorescence planar sensor was compared to the visible image of peat core (side view). The green color of the visual images (Figures 3A, 4A) was from the visual light source (white is not available in the image system used). The corresponding 2-D H<sub>2</sub>S images in Figures 3A, 4A (shown as pseudo-color, reflecting concentrations) revealed that the concentration distribution patterns were directly associated with the plant root structures in marsh peat. The H<sub>2</sub>S concentrations around the roots were <1 mM which was five times less than in the surrounding peat. The results in Figures 3A, 4A were measured in the laboratory in incubated box cores with aeration of overlying seawater for 24 h at room temperature without drainage, the changes of environmental conditions could alter oxygen transport and radial oxygen loss in marsh (Howes and Teal, 1994; Colmer, 2003), as well as H<sub>2</sub>S and Fe<sup>2+</sup> distributions around the roots. In order to avoid these possible artifacts, the real-time 2-D H<sub>2</sub>S and Fe<sup>2+</sup> distribution patterns in salt marshes were studied by deploying the irreversible H<sub>2</sub>S (Yin et al., 2017) and dissolved Fe<sup>2+</sup> (Zhu and Aller, 2012) colorimetric planar sensors *in situ* at different seasons. The real-time data in Figures 5–8A,C showed that the distribution patterns of H<sub>2</sub>S and Fe<sup>2+</sup> in sulfidic marsh

**TABLE 3** | Solid phase organic carbon, total sulfur, chromium reducible sulfide (CRS), acid leachable iron and degree of pyritization (DOP) in the marsh sediments of JoCo and Big Egg, Jamaica Bay, NY.

Marsh Site	Depth (cm)	C (mmol/g)				S ( $\mu\text{mol/g}$ )				CRS ( $\mu\text{mol/g}$ )				Fe ( $\mu\text{mol/g}$ )				DOP*	
		Fall '14	Spring '15	Summer '15	Spring '16	Fall '14	Spring '15	Summer '15	Spring '16	Fall '14	Spring '15	Summer '15	Spring '16	Fall '14	Spring '15	Summer '15	Spring '16	Summer '15	Spring '16
JC1	5	–	26.2	28.4	22.5	–	432	1,040	773	–	–	136	222	–	13.6	12.6	8.0	0.84	0.93
	10	–	24.8	25.8	24.3	–	354	615	907	–	–	121	264	–	9.1	34.1	8.9	0.64	0.94
	15	–	23.8	25.1	27.4	–	344	649	829	–	–	84	154	–	4.8	43.5	5.2	0.49	0.94
	25	–	24.2	20.6	24.7	–	379	715	836	–	–	117	178	–	15.6	43.6	4.4	0.57	0.95
JC2	5	0.36	15.1	23.9	18.2	514	202	660	425	–	–	48	86	–	42.0	126	25.4	0.16	0.63
	10	0.51	17.4	16.0	18.7	496	266	452	694	–	–	127	571	–	24.8	100	10.8	0.39	0.96
	15	0.27	13.6	16.3	11.2	5,412	220	517	464	–	–	194	81	–	33.7	124	44.1	0.44	0.48
	25	1.03	9.8	17.2	15.7	850	209	806	609	–	–	252	333	–	39.8	163	31.9	0.44	0.84
JC3	5	0.24	24.1	23.9	22.2	749	365	724	522	–	–	63	20	–	9.5	19.4	7.1	0.62	0.59
	10	0.47	25.1	22.5	26.9	602	318	647	824	–	–	27	179	–	3.3	13.8	6.1	0.49	0.94
	15	0.11	20.7	25.6	21.8	668	330	530	747	–	–	83	179	–	5.8	9.6	6.8	0.81	0.93
BE1	5	–	7.6	0.27	2.48	–	372	31	504	–	–	8	212	–	78.9	13.5	76.7	0.23	0.58
	10	–	–	0.05	3.10	–	–	15	520	–	–	18	242	–	121.1	5.5	73.6	0.62	0.62
	15	–	5.4	2.3	8.6	–	584	427	711	–	–	166	722	–	156.5	70.7	81.6	0.54	0.82
	25	–	–	5.1	12.1	–	–	1,029	1,970	–	–	418	590	–	–	71.7	–	–	–
BE2	5	1.70	10.0	3.3	12.3	119	350	170	1,080	–	–	157	343	–	67.6	29.7	98.4	0.73	0.64
	10	5.91	15.8	3.5	8.0	402	853	264	418	–	–	193	160	–	198.6	22.0	60.0	0.81	0.57
	15	7	11.0	2.3	6.8	525	668	149	791	–	–	82	461	–	158.4	22.0	93.4	0.65	0.71
	25	–	–	1.1	2.7	–	–	100	290	–	–	73	85	–	–	19.9	30.0	–	–
BE3	5	8.25	11.0	8.4	7.7	654	436	647	819	–	–	355	383	–	68.3	104	127	0.63	0.60
	10	6.30	6.0	8.4	6.9	728	256	475	894	–	–	244	396	–	49.4	49.5	78.3	0.71	0.72
	15	5.95	6.1	4.4	7.0	620	150	252	831	–	–	192	577	–	45.3	43.9	93.6	0.69	0.76
	25	4.67	4.0	3.2	5.6	560	69	272	693	–	–	150	226	–	21.2	44.6	92.8	0.63	0.55

– Indicates not analyzed.

pore water were significantly complicated by belowground radial oxygen loss from roots into the surrounding marsh peat. The oxygen leaked from the roots formed a thin oxic layer in which the dissolved  $\text{H}_2\text{S}$  and  $\text{Fe}^{2+}$  were oxidized to sulfate and Fe-oxide (e.g., iron plaque), resulting in a thin zone of low levels of  $\text{H}_2\text{S}$  and  $\text{Fe}^{2+}$  surrounding the roots in the sulfidic peat. Furthermore, oxygen and/or nitrate, rather than sulfate, served as the electron acceptors for organic matter remineralization in the thin oxic layers. Such an interface of oxic-anoxic sediment around the roots can be seen in both visible peat images and 2-D  $\text{H}_2\text{S}$  images, indicating heterogeneous remineralization patterns. The low and/or undetectable spots/tracks (cold spots) of  $\text{H}_2\text{S}$  and  $\text{Fe}^{2+}$  associated with root structures in **Figures 3–8A,C** was a direct evidence for our hypothesis, and the cold spots of  $\text{H}_2\text{S}$  and  $\text{Fe}^{2+}$  surrounding individual roots became more pronounced (**Figures 7, 8**) when more oxygen transport and high oxygen leakage occurred in the summer season (Colmer, 2003; Soana and Bartoli, 2013).

$\text{H}_2\text{S}$  is a phytotoxin to marsh plants, with a the threshold that can be harmful to *S. alterniflora* of about 2 mM [see Kolker (2005) and references therein]. Long-term exposure of the marsh plants to high levels of  $\text{H}_2\text{S}$  can cause plant die-off and marsh peat collapse. We noted that the average  $\text{H}_2\text{S}$  levels at JoCo marsh could be >4 mM just below the marsh surface (**Figures 4A,B**) or in deep peat (**Figure 7A, JC1**) in the

fall and summer seasons, but JoCo is considered as a “healthy” marsh and plants grow well. We hypothesize that the oxic layers formed around roots of *S. alterniflora* help the plants survive in the high levels of  $\text{H}_2\text{S}$  by reducing sulfide absorption. We tested this hypothesis at the National Synchrotron Light Source-II (Brookhaven National Laboratory; Feng et al., 2018). We used the Hard X-ray Nanoprobe Beamline to obtain nanometer-scale measurements of trace elements in *S. alterniflora* root tissue. The results showed that when iron concentrations in pore water and root epidermis were high, the root epidermis showed lower concentrations of S and P even though sulfide and phosphate in the pore water were high in late summer (Feng et al., 2018). At the same time, pore water Fe was lower than in the spring sampling, but Fe in the root epidermis was high. This pattern is consistent with the roots producing an oxic microenvironment with oxygen transported into the peat through the roots, such that  $\text{Fe}^{2+}$  in the pore water is oxidized, producing iron “plaque” (i.e.  $\text{FeOOH}$ ) on the root epidermis. This plaque prevents sulfide from entering the root tissue. Phosphate may also be excluded *via* adsorption onto the  $\text{FeOOH}$  or formation of an iron phosphate phase.

There are also many “hot spots” on the 2-D  $\text{Fe}^{2+}$  and  $\text{H}_2\text{S}$  images, reflecting the heterogeneous distributions of labile organic matter and the microniches of exoenzymes and microbes on sediment particles (Cao et al., 2013). We also noted that large variation of  $\text{H}_2\text{S}$  and/or  $\text{Fe}^{2+}$  distributions may occur in same

site in duplicate *in situ* measurements over distances of <1 m between two deployed sensor sheets.

In addition to the microscale heterogeneities of  $\text{Fe}^{2+}$  and  $\text{H}_2\text{S}$  distributions around plant roots, the 2-D  $\text{H}_2\text{S}$  and  $\text{Fe}^{2+}$  images also showed clear vertically and laterally heterogeneous distribution patterns. Note that no infaunal burrows were found in the measurements, suggesting that bioturbation is not a factor in these sediments.  $\text{H}_2\text{S}$  concentrations near the surface of the Big Egg sediment were relatively low but sharply increased below the water-sediment interface and reached maxima at  $\sim 2$  cm in the fall sampling at BE1 and BE3. The  $\text{H}_2\text{S}$  levels at JoCo marsh were elevated to 4–6 mM just below the marsh surface (Figures 4A,B). It should be pointed out that the 2-D  $\text{H}_2\text{S}$  distributions in the fall 2014 season (Figures 3A, 4A) were incubated and measured in laboratory with the box core incubation without water drainage, but in all other sampling seasons, the  $\text{H}_2\text{S}$  measurements were performed *in situ* in the field. The real-time 2-D  $\text{H}_2\text{S}$  distributions (Figures 5A, 6A, 7A, 8A) showed that  $\text{H}_2\text{S}$  levels in top 4 cm were low even in the summer season, and gradually increased to higher concentrations at depth. The high  $\text{H}_2\text{S}$  levels elevated just below the water-peat interface in Figure 3A (BE3) and Figure 4A (JC) were not found in the 2-D *in situ* measurements in the field. This phenomenon is likely caused by the pore water drainage in the marshes. The marshes of Jamaica Bay are periodically (tidally) submerged by seawater. An important pathway by which this water drains from marsh islands such as Big Egg and JoCo is vertically, and the two sites have distinctly different drainage velocities of 7.9 and 25.9 cm/d, respectively, as determined by Ra isotopes (Tamborski et al., 2017). Thus the concentrations of  $\text{H}_2\text{S}$  (and other solutes) in marsh peat pore water result from a balance between the rates of biogeochemical processes that produce or consume them and drainage. In summer and fall seasons, higher  $\text{H}_2\text{S}$  concentrations in JC marsh were produced due to the high sulfate-reduction bacteria activities and the relative high organic carbon concentration in this site (Table 3), but the more rapid drainage there produced high flow-through fluxes of  $\text{H}_2\text{S}$  through the marsh peat (Tamborski et al., 2017). As well, the effects of roots on the 2-D  $\text{H}_2\text{S}$  distribution patterns, are especially evident at JC in the summer, a time when marsh plant growth is dense and bacterial activity is high (Figure 7A).

2-D  $\text{Fe}^{2+}$  distributions were measured only by *in situ* sensor deployments, so visible images of the sensing marsh peat were not available. The spatially heterogeneous 2-D  $\text{Fe}^{2+}$  distributions also showed sharp vertical gradients that were closely correlated to the  $\text{H}_2\text{S}$  vertical distributions, especially in the low drainage BE marsh peats.  $\text{Fe}^{2+}$  concentration sharply increased just below the water-sediment interface and reached  $\text{Fe}^{2+}$  maximum zone at 1–2 cm deep. At depths below which the reactive particulate Fe-oxide had been depleted, sulfate reduction dominated the metabolism, producing dissolved sulfide species ( $\text{H}_2\text{S}$ ,  $\text{HS}^-$ , and  $\text{S}^{2-}$ ), and an increase of  $\text{H}_2\text{S}$  with depth in pore water below the  $\text{Fe}^{2+}$  maximum zone (Bull and Taillefert, 2001; Jørgensen and Kasten, 2006; Johnston, 2011). The free sulfide subsequently scavenged the dissolved  $\text{Fe}^{2+}$  to form the reactive solid phase FeS, resulting in a  $\text{Fe}^{2+}$  maximum above the  $\text{H}_2\text{S}$  maximum zone in pore water (Bull and Taillefert, 2001). FeS is unstable and converts

to the more stable form pyrite ( $\text{FeS}_2$ ) by a variety of pathways (Howarth, 1979; Berner, 1984).

The *in situ* zonations of 2-D  $\text{Fe}^{2+}$  and  $\text{H}_2\text{S}$  distributions in Figures 3–8 clearly showed this sequence: the maximum zones of  $\text{Fe}^{2+}$  were generally produced at 2–4 cm, and the  $\text{H}_2\text{S}$  levels increased to maxima below 4 cm. The *in situ* heterogeneous 2-D  $\text{Fe}^{2+}$  and  $\text{H}_2\text{S}$  distributions are useful for determining redox zonation and understanding the dominant biogeochemical processes occurring within the marsh peat. Both dissolved  $\text{Fe}^{2+}$  and  $\text{H}_2\text{S}$  can be efficiently removed by  $\text{FeS}_2$  precipitation from pore water. When millimolar levels of  $\text{H}_2\text{S}$  occurred in marsh pore water, the dissolved  $\text{Fe}^{2+}$  concentrations were generally <20  $\mu\text{M}$  at the same depths. On the other hand, the high pore water concentrations of  $\text{Fe}^{2+}$  were linked to low  $\text{H}_2\text{S}$  levels in all seasons. There were some  $\text{Fe}^{2+}$  “cold spots” co-distributed with low levels of  $\text{H}_2\text{S}$ , as seen in Figures 7A,C. As noted above, these cold spots are likely produced in the oxic and suboxic layers around roots and caused by  $\text{O}_2$  transport down to the deep sediment through the rhizosphere. Unfortunately,  $\text{H}_2\text{S}$  and  $\text{Fe}^{2+}$  concentrations could not be simultaneously measured by optical sensor in the present study.  $\text{Fe}^{2+}$  concentrations at JC and BE were in the range of 10–100  $\mu\text{M}$ , which is typical of coastal marsh pore water. High levels of  $\text{Fe}^{2+}$  in pore water may be harmful to plants because it may co-precipitate or adsorb the nutrients ammonium and phosphate in the marsh, preventing their uptake by the roots.

## Seasonal Variation of $\text{H}_2\text{S}$ and $\text{Fe}^{2+}$ Distributions in Marsh Pore Water

$\text{H}_2\text{S}$  distributions in marsh pore water at all sites varied seasonally, generally with higher  $\text{H}_2\text{S}$  levels in summer and fall, and lower or undetectable levels in spring (Table 2 and Figures 3–8). At the JoCo marsh sites, dissolved  $\text{H}_2\text{S}$  in pore water was <0.02 mM found by sensors in the spring sensor deployments but it was elevated to as high as 3–6 mM in summer and fall at the same sampling sites. Thus was likely due to loadings of labile organic matter on the marshes produced in the summer in the eutrophic Bay, coupled with the temperature-dependent variation of the rate of microbial decomposition of organic matter. The discrete pore water samples showed the redox potential at JoCo from 5 to 15 cm was in the range of –41 to –200 mV in spring while it was lower, –180 to –350 mV, in summer and fall seasons, indicating less “reducing” environments in the marsh peat in the spring (Table 1). Our previous study showed that the exoenzymes and microbes in marine sediments have high activities in the summer and fall, but very low in winter and early spring (Cao et al., 2013). Thus, the temperature dependence of  $\text{H}_2\text{S}$  distributions was a direct reflection of the change in sulfate-reduction microbial activity with temperature. However, data in Table 1 also showed a clear spatial heterogeneity of the redox potential at different marsh sites in the spring season. Relative lower redox potentials were found at Big Egg marsh sites in the spring compared to fall, the reason for this unusual phenomenon was not clear, but the stronger “reducing” conditions at BE resulted in high  $\text{H}_2\text{S}$  levels in the late spring (April–May) (Figure 6A), and as a consequence, likely caused

more plant die-off and marsh loss. H<sub>2</sub>S distributions at BE sites in winter and early spring were not measured.

Typically, the high concentration of H<sub>2</sub>S (or ΣH<sub>2</sub>S) in anaerobic salt marshes comes from the reduction of sulfate during organic matter decomposition, generating a decreasing redox potential with depth (Hambrick III, DeLaune and Patrick, 1980), and a complicated 3-D pattern associated with the roots of plants due to oxygen transport and radial oxygen loss through roots. The redox potential can be used as an indicator of the degree of oxidation of marsh peat. The results in **Table 1** showed that the redox potentials of all sites generally decreased from 5 to 25 cm depth, but exhibited a clear seasonal variation. The redox potential in spring was much higher than that in summer and fall in JC, indicating the lower organic matter oxidation rate by sulfate in spring. The pH values of all sites and depths in summer and fall seasons are in the range of pH 6–7 with vague seasonal variations, implying that the intense oxidation of organic matter by various electron acceptors at warm temperature tend to buffer sediment pore water close to 6–7. Interestingly, the pH values of pore water at JC in spring are in the range of 5–6.5 which are lower than the pH values in other seasons. By integrating other geochemical parameters found at this site in spring, for example the high redox potentials (**Table 1**), extreme low total sulfide (**Table 2**) and non-detectable (<0.02 mM) dissolved H<sub>2</sub>S (**Figure 5A**), we conclude that the rate of organic matter decomposition in JC in late spring (April–May) is still high, but oxidants with high redox potentials (such as O<sub>2</sub>, nitrate, and Mn/Fe-oxides), rather than sulfate, dominate the redox reactions with organic matter at JC. This might be attributed to the healthy and high-density biomass of *S. alterniflora* and fast pore water drainage velocity in JC. The intertidal nature and fast drainage of the JC salt marsh could result in surface gas exchange playing a more important role in the sediment oxygen transports than in low drainage marshes like BE, resulting in a relatively higher redox potential in JC than BE in the spring season.

Fe<sup>2+</sup> concentrations in marsh pore water also show seasonal changes (**Table 2** and **Figures 3C–8C**), but the seasonal changes are not very significant compared to the H<sub>2</sub>S distribution variations, partially due to the low Fe<sup>2+</sup> concentrations in the marsh pore water. But, the distribution patterns of Fe<sup>2+</sup> are closely associated with H<sub>2</sub>S distribution patterns in marsh pore water, as discussed above. It seems that Fe<sup>2+</sup> concentrations in pore water at most sites of JoCo and Big Egg were relatively high in summer than in spring and fall.

The seasonal variation of H<sub>2</sub>S and Fe<sup>2+</sup> in marsh pore water should also be tightly linked to the plant life cycle. The previous studies have shown that the temporal changes in belowground biogeochemical processes, such as oxygen leakages from roots, sulfate reduction, sulfide oxidation, Fe<sup>2+</sup> oxidation and precipitation etc., were well correlated with the changes in plant physiology (Hines et al., 1989; Soana and Bartoli, 2013; LaFond-Hudson et al., 2018). We did not measure directly the oxygen leakage from roots in this study, but the microscale “cold spots” of H<sub>2</sub>S and Fe<sup>2+</sup> in the 2-D distribution patterns associated with individual roots (**Figures 3–8A,C**) clearly indicated radial oxygen loss from roots. In the spring season, low temperatures decreased oxygen consumption in plant rhizosphere by slowing

respiration in roots (Armstrong, 1979), resulting in more “excess” oxygen leakage into surrounding marsh peat and the increase of redox potential in sediment. This could be another possible explanation as to why the redox potential in JC marsh is higher in spring than other seasons (**Table 1**). In the summer season, dissolved organic matter could be released from the roots during active growth of *S. alterniflora* and rapidly enhance the sulfate reduction rate (Hines et al., 1989). We believe that any additional dissolved organic matter released from roots would also fuel the rate of Fe-oxide reduction, resulting in a relative high dissolved Fe<sup>2+</sup> in marsh pore water (**Figures 7C, 8C**). As a consequence, more active FeS was formed and accumulated in summer season in JC (**Table 3**).

### Interaction of H<sub>2</sub>S and Fe<sup>2+</sup> as Seen in the Solid Phase: Degree of Pyritization

The precipitation of the solid phases FeS and FeS<sub>2</sub> (pyrite) as a result of elevated concentrations of H<sub>2</sub>S and Fe<sup>2+</sup> in the pore water effectively removes H<sub>2</sub>S from solution, and is thus a geochemical means of controlling H<sub>2</sub>S concentrations (Howarth, 1979; Berner, 1984). The pore water data described in sections “Heterogeneities of Fe<sup>2+</sup> and H<sub>2</sub>S Distributions in Salt Marsh Pore Water” and “Seasonal Variation of H<sub>2</sub>S and Fe<sup>2+</sup> Distributions in Marsh Pore Water” are essentially snapshots of conditions at the time of sampling. The composition of the solid phase can integrate the redox reactions occurring in the sediments over longer periods. We measured fractions of the solid phase S and Fe pools in the peat at all the sites (**Table 3**). For sulfur, the important pools include Acid Volatile Sulfide (AVS), CRS, and Total Sulfur. AVS is a measure of FeS-associated sulfur, CRS of the pyrite-associated sulfur and total S of the AVS, CRS, and all other forms, including organosulfur compounds. For iron, we measured a fraction termed “reactive” Fe, i.e. that obtained by a 1 N HCl cold leach of the dried sediment. This procedure extracts the portion of Fe that is diagenetically mobile and readily able to react with sulfide to produce the iron sulfide phases. Our prior experience in JoCo (Cochran et al., 2013) suggests that AVS < CRS ≤ Total S. The AVS pool is labile and converts to pyrite, which is a longer term sink for Fe and especially S in the marsh peat. In effect, the formation of pyrite removes dissolved sulfide from the pore water and stores it, lowering the exposure of the plants to this phytotoxin. The solid phase measurements enable calculation of a parameter termed the “Degree of Pyritization” (DOP), that is, the degree to which reactive Fe in the solid phase is associated with pyrite and is thus unable to further remove dissolved sulfide from pore water. DOP is defined as:

$$DOP = \frac{Fe_{pyrite}}{Fe_{pyrite} + Fe_{reactive}} \quad (1)$$

where Fe<sub>pyrite</sub> is calculated as CRS/2 (i.e. one mole of Fe per two moles of S in FeS<sub>2</sub>), and Fe<sub>reactive</sub> is the acid leachable Fe. **Table 3** gives the solid phase DOP results.

The results in **Table 3** show that the total sulfur at JoCo is generally higher than that at Big Egg, but the CRS-sulfur concentrations are comparable at these two sites and the fraction

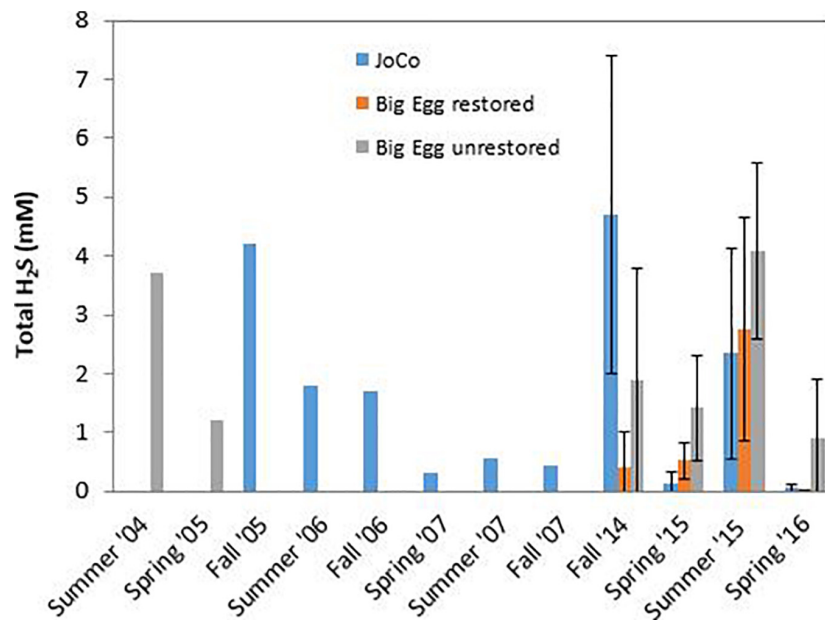


**FIGURE 9 |** Temporal variation of average total dissolved inorganic sulfide ( $\Sigma\text{H}_2\text{S}$ ) in pore water of JoCo and Big Egg salt marsh at Jamaica Bay. BE1 is the restored marsh, BE2 and BE3 are the unrestored marsh. Data were averaged from  $\Sigma\text{H}_2\text{S}$  concentrations measured on samples taken at 4–5 discrete depths from 5 to 30 cm. Vertical lines demote  $1\sigma$  uncertainties of the mean of several sites sampled in each marsh from 2014 to 2016.

of CRS in the total sulfur pool is much smaller in JoCo. To the extent that total sulfur includes diagenetically produced organosulfur compounds and sulfur associated with the marsh plants, this difference can be explainable by the higher organic content of the marsh sediments at JoCo. Both total sulfur and CRS-sulfur show vertical variations at different depths from surface to deep marsh peat, but the pattern at each site is not consistent even in the same season, implying significant heterogeneities of both organosulfur and pyrite-associated sulfur in the solid marsh peat, probably caused by the plant growth. Similar to dissolved  $\text{H}_2\text{S}$  and  $\text{Fe}^{2+}$  in pore water, the total sulfur, CRS-sulfur and acid leachable Fe in the peat also show seasonal differences between the summer 2015 and spring 2016 samplings. These reflect the redox cycling of the various pools of Fe and S over the year.

The DOP at JoCo is higher than that at Big Egg. Indeed, the DOP values at JoCo can approach 1, indicating that 100% of the reactive iron is associated with pyrite. These high values suggest that the biogeochemical control of pore water  $\text{H}_2\text{S}$  via  $\text{FeS}_2$  precipitation is close to a limit and that high sulfide but low  $\text{Fe}^{2+}$  concentrations in the pore water can be expected, as observed.

### Time Series of $\Sigma\text{H}_2\text{S}$ in JoCo and Big Egg Marshes: 2014–2016

Our group has studied Jamaica Bay marshes since 2004 (Cochran et al., 2013, 2018). In particular, we have pore water  $\Sigma\text{H}_2\text{S}$  concentrations measured by “sipper” at the two marshes studied here. All samples were taken in the upper 25–30 cm and analyzed for  $\Sigma\text{H}_2\text{S}$  as described above. Analytical techniques were the same throughout and thus the values are comparable within and

between the marshes. However, although sampling sites were in the same general area of each marsh, they were not identical over time. In addition, not all marsh sites were sampled in each year. The record of sampling includes: Big Egg- 2004/05, 2014–2016; JoCo- 2005–2007, 2014–2016. These time series of samples permit us to examine changes in the average concentration of  $\Sigma\text{H}_2\text{S}$  in pore water of the marsh peat in a depth zone in which root density is high and the plants can be considered susceptible to exposure to elevated levels of his phytotoxin. To do this, we calculated the average  $\Sigma\text{H}_2\text{S}$  value of the pore water analyses from sippers deployed from ~5 to 30 cm. Generally, 4–5 sample depths were involved (e.g., 5, 10, 15, and 25 cm). All sites sampled in each marsh at a given time were averaged to produce a single  $\Sigma\text{H}_2\text{S}$  value, presumed to be representative of that marsh at that time. The results are shown in **Figure 9**, and the patterns in each marsh are as follows:

**Big Egg:** a portion of this marsh (BE1) was restored in 2003 by spraying sandy sediment from the adjacent subtidal bottom onto the marsh surface (Frame et al., 2006). The unrestored portion of the marsh was sampled in 2004/05 and again in our recent sampling. We also sampled the restored portion of the marsh in the present study (BE1). The effects of the sediment spray are well documented in the  $^{210}\text{Pb}$  profile in the core taken in this area of the marsh (Cochran et al., 2018; data not shown). Concentrations of  $\Sigma\text{H}_2\text{S}$  in the unrestored portion of the marsh are as high as 3.5–4 mM in the summer and are quite similar between 2004/05 and 2014–16, with comparable values in comparable seasons (**Figure 9**). Samples from the restored portion of the marsh appear to have lower  $\Sigma\text{H}_2\text{S}$  in the pore water, and the offset is especially clear in the fall 2014, and spring 2015 and 2016 samplings.

**JoCo:** JoCo presents a conundrum in that it is considered a “healthy” marsh in Jamaica Bay, yet over the period 2005–2016, average  $\Sigma\text{H}_2\text{S}$  levels were  $>2$  mM in summer and fall, 2006 and summer, 2015 and exceeded 4 mM in fall, 2005 and 2014. Offsetting these high concentrations is the fact that levels of  $\Sigma\text{H}_2\text{S}$  were low ( $<0.5$  mM) at other sampling times, including in the spring, summer and fall, 2007, and were exceptionally low ( $\sim 0$  mM) in spring, 2015 and 2016. Several factors controlling  $\Sigma\text{H}_2\text{S}$  are likely in play at JoCo. The large variations in  $\Sigma\text{H}_2\text{S}$  from sampling to sampling may in part be due to the fact that most of the reactive iron in the JoCo peat is associated with  $\text{FeS}_2$  and is thus not able to readily react with  $\text{H}_2\text{S}$  produced *via* sulfate reduction. Secondly, although temperature is a strong control on bacterial activity and hence the production of  $\text{H}_2\text{S}$ , there is no clear relationship between mean air temperature during the month or week of sampling and mean pore water  $\Sigma\text{H}_2\text{S}$  (data not shown). As noted above, drainage rates in JoCo are the fastest seen of the marshes examined in this study (Tamborski et al., 2017). These rates may vary with time as a function of tides (neap vs. spring) and season (warm vs. cold; variation in precipitation). It is possible that at least the portion of JoCo studied is at or near a “tripping point” for degradation.

## CONCLUSION

Pore water  $\text{H}_2\text{S}$  and  $\text{Fe}^{2+}$  distributions were measured at Big Egg and JoCo marshes in Jamaica Bay using *in situ* optical sensors that produced 2-D images of concentrations. Both  $\text{H}_2\text{S}$  and  $\text{Fe}^{2+}$  distributions showed significant vertical and horizontal heterogeneities, as well as seasonal variations. The complicated 2-D distribution patterns associated with the effects of roots (e.g., oxygen transport) were also revealed. The sensor measurements were generally in good agreement with the dissolved  $\text{H}_2\text{S}$  values obtained from discrete pore water samples (calculated from  $\Sigma\text{H}_2\text{S}$  and pH). However, the dissolved  $\text{Fe}^{2+}$  data obtained from the discrete pore water samples were somewhat less than those from *in situ* sensor measurements. In particular, the traditional discrete method missed the  $\text{Fe}^{2+}$  maximum zones and spatial resolution of  $\text{Fe}^{2+}$  in the marsh pore water. The  $\text{H}_2\text{S}$  concentrations measured by *in situ* sensors at JoCo and Big Egg were elevated (2–6 mM) in late summer and early fall, but show a clear seasonal difference. The elevated  $\text{H}_2\text{S}$  levels were higher than the threshold at which adverse effects on marsh plants may occur ( $\sim 2$  mM). On the other hand, oxic zones formed around roots likely protect the plants from absorbing  $\text{H}_2\text{S}$  in an extreme sulfidic environment. Dissolved  $\text{Fe}^{2+}$  concentrations in pore water measured with sensors at Big Egg and JoCo are generally low, largely due to the removal by pyritization. The data of solid phase S and Fe at Big Egg and JoCo showed that significant amounts ( $>50\%$ ) of diagenetically reactive Fe were associated with the pyrite and thus not readily able to react as pore water  $\text{H}_2\text{S}$  increases. Indeed, at JoCo, virtually all of the reactive Fe was associated with pyrite in the spring, 2016 sampling, suggesting that the negative feedback on pore water  $\text{H}_2\text{S}$  concentrations associated with the coupled Fe and S redox cycles is weak and that the ability

of Fe to control pore water sulfide through pyrite formation is limited there.

The present study, together with those conducted by our group since 2004, has permitted us to document the pore water geochemistry of the Big Egg and JoCo. The large change is seen in the significant reduction of the phytotoxin  $\text{H}_2\text{S}$  in the pore water in the restored portion of Big Egg marsh, while the unrestored portions there continue to display high pore water  $\text{H}_2\text{S}$ , especially in summer samplings. At JoCo, sampling in fall, 2005, and summer and fall, 2006 showed high (2–4 mM) average values of  $\text{H}_2\text{S}$  in the pore water. In contrast values in spring, summer and fall, 2007 were  $<0.5$  mM. The recent sampling in 2014–16 shows strong seasonality, with high values in fall, 2014 ( $>4$  mM) and summer, 2015, but low values ( $<0.2$  mM) in the two spring samplings (2015, 2016). Although the marsh plants at JoCo are exposed to occasional high levels of  $\text{H}_2\text{S}$  that might be considered toxic, the marsh is relatively elevated compared with mean sea level, and drainage through the marsh peat is more rapid at JoCo than at Big Egg. This may help explain why JoCo continues to be a “healthy” marsh. Relatively healthy marshes such as JoCo should especially be the subject of continued monitoring, for both geochemical and biological parameters.

## DATA AVAILABILITY STATEMENT

The original contributions presented in the study are included in the article/supplementary material, further inquiries can be directed to the corresponding author/s.

## AUTHOR CONTRIBUTIONS

QZ and JC: conceived of the project. QZ, JC, CH, HY, HF, JT, PF, and WC: pore water and marsh peat cores sampling in the field. QZ and HY: field and lab sensor deployments and analyses. CH and JC: pore water and sediment analyses in field and lab. QZ, JC, and CH: data interpretation and manuscript preparation. All authors contributed to the article and approved the submitted version.

## FUNDING

This work was supported by funding from the National Park Service (Task Agreement P14AC01395, Cooperative Agreement P14AC00888). The sensors were partially support by NSF OCE 1737749 and NSF OCE 1332418.

## ACKNOWLEDGMENTS

We would like to thank the Science and Resilience Institute at Jamaica Bay for supporting field work, Robert C. Aller for discussion of results, Yu Qian for assistance in the field. Patricia Rafferty (National Parks Service) Don Riepe, and Elizabeth Manclark (American Littoral Society) provided much appreciated logistical support.

## REFERENCES

- Allred, M., Borrelli, J. J., Hoellein, T., Bruesewitz, D., and Zarnoch, C. (2020). Marsh plants enhance coastal marsh resilience by changing sediment oxygen and sulfide concentrations in an urban, eutrophic estuary. *Estuaries Coasts* 43, 801–813. doi: 10.1007/s12237-020-00700-9
- Aller, R. C. (1982). “The effects of macrobenthos on chemical properties of marine sediments and overlying water,” in *Animal-Sediment Relations*, eds P. L. McCall and M. J. S. Tevesz (New York, NY: Plenum), 53–102. doi: 10.1007/978-1-4757-1317-6\_2
- Aller, R. C. (2001). “Transport and reactions in the bioirrigated zone,” in *The Benthic Boundary Layer*, eds B. P. Boudreau and B. B. Jørgensen (Oxford: Oxford University Press), 269–301.
- Aller, R. C., Madrid, V., Chistoserdov, A., Aller, J. Y., and Heilbrun, C. (2010). Unsteady diagenetic processes and sulfur biogeochemistry in tropical deltaic muds: implications for oceanic isotope cycles and the sedimentary record. *Geochim. Cosmochim. Acta* 74, 4671–4692. doi: 10.1016/j.gca.2010.05.008
- Armstrong, W. (1979). Aeration in higher plants. *Adv. Bot. Res.* 7, 225–332. doi: 10.1016/s0065-2296(08)60089-0
- Bagarinao, T. (1992). Sulfide as an environmental factor and toxicant–tolerance and adaptations in aquatic organisms. *Aquat. Toxicol.* 24, 21–62. doi: 10.1016/0166-445x(92)90015-f
- Berner, R. A. (1970). Sedimentary pyrite formation. *Am. J. Sci.* 268, 1–23. doi: 10.2475/ajs.268.1.1
- Berner, R. A. (1984). Sedimentary pyrite formation: an update. *Geochim. Cosmochim. Acta* 48, 605–615. doi: 10.1016/0016-7037(84)90089-9
- Brendel, P., and Luther, G. W. (1995). Development of a gold amalgam voltammetric microelectrode for the determination of dissolved Fe, Mn, O<sub>2</sub> and S(-2) in pore waters of marine and freshwater sediments. *Environ. Sci. Technol.* 29, 751–761. doi: 10.1021/es00003a024
- Bull, D. C., and Taillefert, M. (2001). Seasonal and topographic variations in pore waters of a southeastern USA salt marsh as revealed by voltammetric profiling. *Geochem. Trans.* 2, 104. doi: 10.1039/b108493c
- Campbell, A., Wang, Y., Christiano, M., and Steverns, S. (2017). Salt Marsh Monitoring in Jamaica Bay, New York from 2003 to 2013: a decade of change from restoration to hurricane sandy. *Remote Sens.* 9:131. doi: 10.3390/rs9020131
- Canfield, D. E. (1989). Reactive iron in marine sediments. *Geochim. Cosmochim. Acta* 53, 619–632. doi: 10.1016/0016-7037(89)90005-7
- Canfield, D. E., Raiswell, R., and Bottrell, S. (1992). The reactivity of sedimentary iron minerals toward sulfide. *Am. J. Sci.* 292, 659–683. doi: 10.2475/ajs.292.9.659
- Cao, Z., Zhu, Q., Aller, R. C., Aller, J. Y., and Waugh, S. (2013). Seasonal, 2-D sedimentary extracellular enzyme activities and controlling processes in Great Peconic Bay. *Long Island. J. Mar. Res.* 71, 399–423. doi: 10.1357/002224013812587573
- Cline, J. E. (1969). Spectrophotometric determination of hydrogen sulfide in natural waters. *Limnol. Oceanogr.* 14, 454–458. doi: 10.4319/lo.1969.14.3.0454
- Cochran, J. K., Kolker, A. S., Hirschberg, D. J., Renfro, A. A., Goodbred, S. Jr., and Beck, A. J. (2013). *Sulfur Cycling in Salt Marshes of Jamaica Bay, Gateway National Recreation Area: Possible Links to Marsh Loss*. Natural Resource Technical Report NPS/NER/NRTR–2013/730. Fort Collins, CO: National Park Service.
- Cochran, J. K., Zhu, Q., Heilbrun, C., Tamborski, J., Yin, H., Fitzgerald, P., et al. (2018). *Health and Resilience of Salt Marshes in Jamaica Bay, NY: Geochemical and Dynamical Perspectives*. Natural Resources Report NPS/NCBN/NRR – 2018/1643. Fort Collins, CO: National Park Service.
- Colmer, T. D. (2003). Long-distance transport of gases in plants: a perspective on internal aeration and radial oxygen loss from roots. *Plant Cell Environ.* 26, 17–36. doi: 10.1046/j.1365-3040.2003.00846.x
- Deegan, L. A., Johnson, D. S., Warren, R. S., Peterson, B. J., Fleeger, J. W., Fagherazzi, S., et al. (2012). Coastal eutrophication as a driver of salt marsh loss. *Nature* 490, 388–392. doi: 10.1038/nature11533
- Feng, H., Qian, Y., Cochran, J. K., Zhu, Q., Heilbrun, C., Li, L., et al. (2018). Seasonal differences in trace element concentrations and distributions in *Spartina alterniflora* root tissue. *Chemosphere* 204, 359–370. doi: 10.1016/j.chemosphere.2018.04.058
- Frame, G. W., Mellander, M. K., and Adamo, D. A. (2006). “Big egg marsh experimental restoration in Jamaica Bay, New York,” in *People, Places, and Parks: Proceedings of the 2005 George Wright Society Conference on Parks, Protected Areas, and Cultural Sites*, ed. D. Harmon (Hancock, MI: The George Wright Society), 123–130.
- Goldhaber, M. B. (2003). “Sulfur-rich Sediments,” in *Treatise on Geochemistry*, Vol. 7, ed. F. T. Mackenzie (Amsterdam: Elsevier), 257–288. doi: 10.1016/b0-08-043751-6/07139-5
- Hambrick III, G. A., DeLaune, R. D., and Patrick, W. H. (1980). Effect of estuarine sediment pH and oxidation-reduction potential on microbial hydrocarbon degradation. *Appl. Environ. Microbiol.* 40, 365–369. doi: 10.1128/aem.40.2.365-369.1980
- Han, C., Ren, J., Tang, H., Xu, D., and Xie, X. (2016). Quantitative imaging of radial oxygen loss from *Valisneria spiralis* roots with a fluorescent planar optode. *Sci. Total Environ.* 569–570, 1232–1240. doi: 10.1016/j.scitotenv.2016.06.198
- Hines, M. E., Knollmeyer, S. L., and Tugel, J. B. (1989). Sulfate reduction and other sedimentary biogeochemistry in a northern New England salt marsh. *Limnol. Oceanogr.* 34, 578–590. doi: 10.4319/lo.1989.34.3.0578
- Howarth, R. W. (1979). Pyrite: its rapid formation in a salt marsh and its importance in ecosystem metabolism. *Science* 203, 49–51. doi: 10.1126/science.203.4375.49
- Howes, B. L., and Teal, J. M. (1994). Oxygen loss from *Spartina alterniflora* and its relationship to salt marsh oxygen balance. *Oecologia* 97, 431–438. doi: 10.1007/bf00325879
- Johnston, D. T. (2011). Multiple sulfur isotopes and the evolution of Earth’s surface sulfur cycle. *Earth Sci. Rev.* 106, 161–183. doi: 10.1016/j.earscirev.2011.02.003
- Jørgensen, B. B., and Kasten, S. (2006). “Sulfur cycling and methane oxidation,” in *Marine Geochemistry*, eds H. D. Schulz and M. Zabel (Berlin: Springer), 271–309. doi: 10.1007/3-540-32144-6\_8
- Jørgensen, B. B., and Nelson, D. C. (2004). “Sulfide oxidation in marine sediments: geochemistry meets microbiology,” in *Sulfur Biogeochemistry – Past and Present*, Vol. 379, eds J. P. Amend, K. J. Edward, and T. W. Lyons (Boulder, CO: Geological Society of America), 63–81.
- Kolker, A. S. (2005). *The Impacts of Climate Variability and Anthropogenic Activities on Salt Marsh Accretion and Loss on Long Island*. Ph.D. Thesis. Stony Brook, NY: Stony Brook University, 260.
- Koop-Jakobsen, K., Mueller, P., Meier, R. J., Liebsch, G., and Jensen, K. (2018). Plant-sediment interactions in salt marshes – an optode imaging study of O<sub>2</sub>, pH, and CO<sub>2</sub> gradients in the rhizosphere. *Front. Plant Sci.* 9:541. doi: 10.3389/fpls.2018.00541
- Kostka, J. E., and Luther, G. W. (1995). Seasonal cycling of Fe in saltmarsh sediments. *Biogeochemistry* 29, 159–181. doi: 10.1007/bf00000230
- LaFond-Hudson, S., Johnson, N. W., Pastor, J., and Dewey, B. (2018). Iron sulfide formation on root surfaces controlled by the life cycle of wild rice (*Zizania palustris*). *Biogeochemistry* 141, 95–106. doi: 10.1007/s10533-018-0491-5
- Lamers, L. P. M., Govers, L. L., Jassen, I. C. J. M., Geurts, J. J. M., Van der Welle, M. E. W., and Van Katwijk, M. M. (2013). Sulfide as a soil phytotoxin—a review. *Front. Plant Sci.* 4:268. doi: 10.3389/fpls.2013.00268
- Luo, M., Huang, J., Tong, C., Liu, Y., Duan, X., and Hu, Y. (2017). Iron dynamics in a subtropical estuarine tidal marsh: effect of season and vegetation. *Mar. Ecol. Prog. Ser.* 577, 1–15. doi: 10.3354/meps12268
- Luo, M., Zeng, C. S., Tong, C., Huang, J. F., Chen, K., and Liu, F. Q. (2016). Iron reduction along an inundation gradient in a tidalsedge (*Cyperus malaccensis*) marsh: the rates, pathways, and contributions to anaerobic organic matter mineralization. *Estuaries Coasts* 39, 1679–1693. doi: 10.1007/s12237-016-0094-0
- Luo, M., Zeng, C. S., Tong, C., Huang, J. F., Yu, Q., Guo, Y. B., et al. (2015). Kinetics of chemical and microbial iron reduction along an inundation gradient in a tidal marsh of the Min River Estuary, Southeastern China. *Geomicrobiol. J.* 32, 635–647. doi: 10.1080/01490451.2014.950362
- Luther, G. W., and Church, T. M. (1988). Seasonal cycling of sulfur and iron in pore waters of a Delaware salt marsh. *Mar. Chem.* 23, 295–309. doi: 10.1016/0304-4203(88)90100-4
- Luther, G. W., Church, T. M., Scudlark, J. R., and Cosman, M. (1986). Inorganic and organic sulfur cycling in salt-marsh pore waters. *Science* 232, 746–749. doi: 10.1126/science.232.4751.746

- Luther, G. W., Findlay, A. J., MacDonald, D. J., Owings, S. M., Hanson, T. E., Beinart, R. A., et al. (2011). Thermodynamics and kinetics of sulfide oxidation by oxygen: a look at inorganically controlled reactions and biologically mediated processes in the environment. *Front. Microbiol.* 2:62. doi: 10.3389/fmicb.2011.00062
- Marsooli, R., Orton, P. M., and Mellor, G. (2017). Modeling wave attenuation by salt marshes in Jamaica Bay, New York, using a new rapid wave model. *J. Geophys. Res. Oceans* 122, 5689–5707. doi: 10.1002/2016jc012546
- Morse, J. W., Millero, F. J., Cornwell, J. C., and Rickard, D. (1987). The chemistry of the hydrogen sulfide and iron sulfide system in natural water. *Earth Sci. Rev.* 24, 1–42. doi: 10.1016/0012-8252(87)90046-8
- New York City Department of Environmental Protection (2007a). *Jamaica Bay Watershed Protection Plan*, Vol. I. New York, NY: New York City Department of Environmental Protection.
- New York City Department of Environmental Protection (2007b). *Jamaica Bay Watershed Protection Plan*, Vol. II. New York, NY: New York City Department of Environmental Protection.
- NYSDEC (2006). *Tidal Wetland Losses in Jamaica Bay*. Queens County, NY: NYSDEC.
- Rafferty, P., Castagna, J., and Adamo, D. (2010). *Building Partnerships to Restore an Urban Marsh Ecosystem at Gateway National Recreation Area*. Washington, DC: National Park Service.
- Reese, B. K., Finneran, D. W., Mills, H. J., Zhu, M.-X., and Morse, J. W. (2011). Examination and refinement of the determination of aqueous hydrogen sulphide. *Aquat. Geochem.* 17, 567–582. doi: 10.1007/s10498-011-9128-1
- Soana, E., and Bartoli, M. (2013). Seasonal variation of radial oxygen loss in *Vallisneria spiralis* L: an adaptive response to sediment redox? *Aqua. Bot.* 104, 228–232. doi: 10.1016/j.aquabot.2012.07.007
- Stookey, L. L. (1970). Ferrozine – a new spectrophotometric reagent for iron. *Anal. Chem.* 42, 779–781. doi: 10.1021/ac60289a016
- Sundby, B., Vale, C., Caetano, M., and Luther, G. W. (2003). Redox chemistry in the root zone of a salt marsh sediment in the Tagus Estuary, Portugal. *Aquat. Geochem.* 9, 257–271. doi: 10.1023/b:aqua.0000022957.42522.9a
- Tamborski, J. J., Cochran, J. K., Heilbrun, C., Rafferty, P., Fitzgerald, P., Zhu, Q., et al. (2017). Investigation of pore water residence times and drainage velocities in salt marshes using short-lived radium isotopes. *Mar. Chem.* 196, 107–115. doi: 10.1016/j.marchem.2017.08.007
- USFWS (U.S. Fish & Wildlife Service) (1997). *Significant Habitats and Habitat Complexes of the New York Bight Watershed*. Charlestown, RI: U.S. Fish & Wildlife service.
- Weiss, J. V., Emerson, D., and Magonigal, J. P. (2005). Rhizosphere iron (III) deposition and reduction in a *Juncus effusus* L.-dominated wetland. *Soil Sci. Soc. Am. J.* 69, 1861–1870. doi: 10.2136/sssaj2005.0002
- Yin, H., Zhu, Q., and Aller, R. C. (2017). An irreversible planar optical sensor for multi-dimensional measurements of sedimentary H<sub>2</sub>S. *Mar. Chem.* 195, 143–152. doi: 10.1016/j.marchem.2017.03.005
- Zhu, Q., and Aller, R. C. (2012). Two-dimensional dissolved ferrous iron distributions in marine sediments as revealed by a novel planar optical sensor. *Mar. Chem.* 136–137, 14–23. doi: 10.1016/j.marchem.2012.04.002
- Zhu, Q., and Aller, R. C. (2013). Planar fluorescence sensors for two-dimensional measurements of H<sub>2</sub>S distributions and dynamics in sedimentary deposits. *Mar. Chem.* 157, 49–58. doi: 10.1016/j.marchem.2013.08.001

**Conflict of Interest:** The authors declare that the research was conducted in the absence of any commercial or financial relationships that could be construed as a potential conflict of interest.

The handling editor declared a past co-authorship with the authors JC and CH.

Copyright © 2021 Zhu, Cochran, Heilbrun, Yin, Feng, Tamborski, Fitzgerald and Cong. This is an open-access article distributed under the terms of the Creative Commons Attribution License (CC BY). The use, distribution or reproduction in other forums is permitted, provided the original author(s) and the copyright owner(s) are credited and that the original publication in this journal is cited, in accordance with accepted academic practice. No use, distribution or reproduction is permitted which does not comply with these terms.